https://ntrs.nasa.gov/search.jsp?R=19840007467 2020-03-21T01:35:56+00:00Z

## General Disclaimer

## One or more of the Following Statements may affect this Document

- This document has been reproduced from the best copy furnished by the organizational source. It is being released in the interest of making available as much information as possible.

- This document may contain data, which exceeds the sheet parameters. It was furnished in this condition by the organizational source and is the best copy available.

- This document may contain tone-on-tone or color graphs, charts and/or pictures, which have been reproduced in black and white.

- This document is paginated as submitted by the original source.

- Portions of this document are not fully legible due to the historical nature of some of the material. However, it is the best reproduction available from the original submission.

Produced by the NASA Center for Aerospace Information (CASI)

NASA CR- 170612

# ANALYSIS OF SHORT PULSE LASER ALTIMETRY DATA OBTAINED OVER HORIZONTAL PATH

by

K. E. Im
B. M. Tsai
C. S. Gardner

RRL Publication No. 526

Technical Report
September 1983

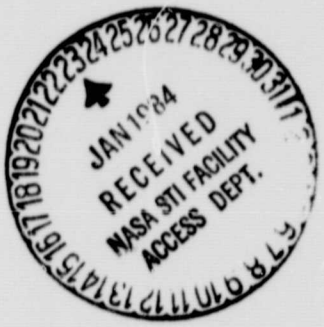


Supported by
Contract No. NASA NSG-5049

NATIONAL AERONAUTICS & SPACE ADMINISTRATION
Goddard Space Flight Center
Greenbelt, Maryland 20771

RADIO RESEARCH LABORATORY
DEPARTMENT OF ELECTRICAL ENGINEERING
COLLEGE OF ENGINEERING
UNIVERSITY OF ILLINOIS
URBANA, ILLINOIS 61801

(NASA-CR-170612) ANALYSIS OF SHORT PULSE LASER ALTIMETRY DATA OBTAINED OVER HORIZONTAL PATH (Illinois Univ.) 79 p
HC A05/MF A01 CSCL 20E G3/36

N84-15535
Unclas
15164

# ANALYSIS OF SHORT PULSE LASER ALTIMETRY DATA OBTAINED OVER HORIZONTAL PATH

by

K. E. Im
B. M. Tsai
C. S. Gardner

RRL Publication No. 526

Technical Report
September 1983

Supported by
Contract No. NASA NSG-5049

NATIONAL AERONAUTICS & SPACE ADMINISTRATION
Goddard Space Flight Center
Greenbelt, Maryland 20771

RADIO RESEARCH LABORATORY
DEPARTMENT OF ELECTRICAL ENGINEERING
COLLEGE OF ENGINEERING
UNIVERSITY OF ILLINOIS
URBANA, ILLINOIS 61801

## ACKNOWLEDGEMENTS

The authors would like to thank Dr. James B. Abshire for his invaluable suggestions and assistance throughout the experiment. Many thanks are also owed to Mrs. Jan McGarry for her help in developing software and Mr. H. E. Rowe for his help in collecting the data.

This work was supported by the National Aeronautics and Space Administration Goddard Space Flight Center, under Contract NASA NSG-5049.

TABLE OF CONTENTS


| | | Page |
|---|---|---|
| 1. | INTRODUCTION. . . . . | 1 |
| 2. | TARGET CONFIGURATONS. . . . . | 2 |
| 3. | SYSTEM HARDWARE . . . . . | 9 |
| 4. | DATA PROCESSING . . . . . | 15 |
| 5. | DATA ANALYSIS . . . . . | 59 |
| 6. | CONCLUSION. . . . . | 64 |
| | REFERENCES. . . . . | 65 |
| | CUMULATIVE LIST OF RADIO RESEARCH LABORATORY REPORTS PREPARED UNDER NASA GRANT NSG-5049 . . . . . | 66 |
| | PAPERS PUBLISHED. . . . . | 68 |

# LIST OF FIGURES


| Figure | | Page |
|---|---|---|
| 1. | Front view of the periscope mirror. . . . . | 5 |
| 2. | Front view of the 36" by 1.5" flat plate target and reference retroreflector. . . . . | 6 |
| 3. | Side view of the 36" by 6" flat plate target and reference retroreflector. . . . . | 7 |
| 4. | Front view of the bicycle reflector array and reference retroreflector. . . . . | 8 |
| 5. | The laser ranging system with the old receiver configuration. . | 10 |
| 6. | New receiver configuration. . . . . | 13 |
| 7. | (a) A typical return waveform which contains both the returns from the bicycle reflector array and the retro-reflector; (b) The same waveform after subtracting the retro-reflector return. . . . . | 17 |
| 8. | Sample waveforms of the received signals after alignment from file P0329A (see parameter descriptions in Table 4) . . . . . | 20 |
| 9. | Mean received signal from file P0329A (see parameter descriptions in Table 4). . . . . | 20 |
| 10. | Standard deviation of the received signals from file P0329A (see parameter descriptions in Table 4) . . . . . | 21 |
| 11. | Signal-to-noise ratio of the received signals from file P0329A (see parameter descriptions in Table 4) . . . . . | 21 |
| 12. | History of the arrival times of the received signals from file P0329A (see parameter descriptions in Table 4). . . . . | 22 |
| 13. | Histogram of the arrival times of the received signals from file P0329A : number of waveforms vs. arrival time (see parameter descriptions in Table 4). . . . . | 22 |
| 14. | Sample waveforms of the received signals after alignment from file P0329B (see parameter descriptions in Table 4) . . . . . | 23 |
| 15. | Mean received signal from file P0329B (see parameter descriptions in Table 4). . . . . | 23 |
| 16. | Standard deviation of the received signals from file P0329B (see parameter descriptions in Table 4) . . . . . | 24 |
| 17. | Signal-to-noise ratio of the received signals from file P0329B (see parameter descriptions in Table 4) . . . . . | 24 |

18. History of the arrival times of the received signals from file P0329B (see parameter descriptions in Table 4). . . . . 25

19. Histogram of the arrival times of the received signals from file P0329B : number of waveforms vs. arrival time (see parameter descriptions in Table 4). . . . . 25

20. Sample waveforms of the received signals after alignment from file P0329C (see parameter descriptions in Table 4) . . . . . 26

21. Mean received signal from file P0329C (see parameter descriptions in Table 4). . . . . 26

22. Standard deviation of the received signals from file P0329C (see parameter descriptions in Table 4) . . . . . 27

23. Signal-to-noise ratio of the received signals from file P0329C (see parameter descriptions in Table 4) . . . . . 27

24. History of the arrival times of the received signals from file P0329C (see parameter descriptions in Table 4). . . . . 28

25. Histogram of the arrival times of the received signals from file P0329C : number of waveforms vs. arrival time (see parameter descriptions in Table 4). . . . . 28

26. Sample waveforms of the received signals after alignment from file P0401A (see parameter descriptions in Table 4) . . . . . 29

27. Mean received signal from file P0401A (see parameter descriptions in Table 4). . . . . 29

28. Standard deviation of the received signals from file P0401A (see parameter descriptions in Table 4) . . . . . 30

29. Signal-to-noise ratio of the received signals from file P0401A (see parameter descriptions in Table 4) . . . . . 30

30. History of the arrival times of the received signals from file P0401A (see parameter descriptions in Table 4). . . . . 31

31. Histogram of the arrival times of the received signals from file P0401A : number of waveforms vs. arrival time (see parameter descriptions in Table 4). . . . . 31

32. Sample waveforms of the received signals after alignment from file P0401B (see parameter descriptions in Table 4) . . . . . 32

33. Mean received signal from file P0401B (see parameter descriptions in Table 4). . . . . 32

34. Standard deviation of the received signals from file P0401B (see parameter descriptions in Table 4) . . . . . 33

35. Signal-to-noise ratio of the received signals from file P0401B (see parameter descriptions in Table 4) . . . . . 33

36. History of the arrival times of the received signals from file P0401B (see parameter descriptions in Table 4). . . . . 34

37. Histogram of the arrival times of the received signals from file P0401B : number of waveforms vs. arrival time (see parameter descriptions in Table 4). . . . . 34

38. Sample waveforms of the received signals after alignment from file P0401C (see parameter descriptions in Table 4) . . . . . 35

39. Mean received signal from file P0401C (see parameter descriptions in Table 4). . . . . 35

40. Standard deviation of the received signals from file P0401C (see parameter descriptions in Table 4) . . . . . 36

41. Signal-to-noise ratio of the received signals from file P0401C (see parameter descriptions in Table 4) . . . . . 36

42. History of the arrival times of the received signals from file P0401C (see parameter descriptions in Table 4). . . . . 37

43. Histogram of the arrival times of the received signals from file P0401C : number of waveforms vs. arrival time (see parameter descriptions in Table 4). . . . . 37

44. Sample waveforms of the received signals after alignment from file P0401D (see parameter descriptions in Table 4) . . . . . 38

45. Mean received signal from file P0401D (see parameter descriptions in Table 4). . . . . 38

46. Standard deviation of the received signals from file P0401D (see parameter descriptions in Table 4) . . . . . 39

47. Signal-to-noise ratio of the received signals from file P0401D (see parameter descriptions in Table 4) . . . . . 39

48. History of the arrival times of the received signals from file P0401D (see parameter descriptions in Table 4). . . . . 40

49. Histogram of the arrival times of the received signals from file P0401D : number of waveforms vs. arrival time (see parameter descriptions in Table 4). . . . . 40

50. Sample waveforms of the received signals after alignment from file P0401E (see parameter descriptions in Table 4) . . . . . 41

51. Mean received signal from file P0401E (see parameter descriptions in Table 4). . . . . 41

52. Standard deviation of the received signals from file P0401E (see parameter descriptions in Table 4) . . . . . 42

53. Signal-to-noise ratio of the received signals from file P0401E (see parameter descriptions in Table 4) . . . . . 42

54. History of the arrival times of the received signals from file P0401E (see parameter descriptions in Table 4). . . . . 43

55. Histogram of the arrival times of the received signals from file P0401E : number of waveforms vs. arrival time (see parameter descriptions in Table 4). . . . . 43

56. Sample waveforms of the received signals after alignment from file T0331A (see parameter descriptions in Table 4) . . . . . 44

57. Mean received signal from file T0331A (see parameter descriptions in Table 4). . . . . 44

58. Standard deviation of the received signals from file T0331A (see parameter descriptions in Table 4) . . . . . 45

59. Signal-to-noise ratio of the received signals from file T0331A (see parameter descriptions in Table 4) . . . . . 45

60. History of the arrival times of the received signals from file T0331A (see parameter descriptions in Table 4). . . . . 46

61. Histogram of the arrival times of the received signals from file T0331A : number of waveforms vs. arrival time (see parameter descriptions in Table 4). . . . . 46

62. Sample waveforms of the received signals after alignment from file T0331B (see parameter descriptions in Table 4) . . . . . 47

63. Mean received signal from file T0331B (see parameter descriptions in Table 4). . . . . 47

64. Standard deviation of the received signals from file T0331B (see parameter descriptions in Table 4) . . . . . 48

65. Signal-to-noise ratio of the received signals from file T0331B (see parameter descriptions in Table 4) . . . . . 48

66. History of the arrival times of the received signals from file T0331B (see parameter descriptions in Table 4). . . . . 49

67. Histogram of the arrival times of the received signals from file T0331B : number of waveforms vs. arrival time (see parameter descriptions in Table 4). . . . . 49

68. Sample waveforms of the received signals after alignment from file T0331C (see parameter descriptions in Table 4) . . . . . 50

69. Mean received signal from file T0331C (see parameter descriptions in Table 4). . . . . 50

70. Standard deviation of the received signals from file T0331C (see parameter descriptions in Table 4) . . . . . 51

71. Signal-to-noise ratio of the received signals from file T0331C (see parameter descriptions in Table 4) . . . . . 51

72. History of the arrival times of the received signals from file T0331C (see parameter descriptions in Table 4). . . . . 52

73. Histogram of the arrival times of the received signals from file T0331C : number of waveforms vs. arrival time (see parameter descriptions in Table 4). . . . . 52

74. Sample waveforms of the received signals after alignment from file T0331D (see parameter descriptions in Table 4) . . . . . 53

75. Mean received signal from file T0331D (see parameter descriptions in Table 4). . . . . 53

76. Standard deviation of the received signals from file T0331D (see parameter descriptions in Table 4) . . . . . 54

77. Signal-to-noise ratio of the received signals from file T0331D (see parameter descriptions in Table 4) . . . . . 54

78. History of the arrival times of the received signals from file T0331D (see parameter descriptions in Table 4). . . . . 55

79. Histogram of the arrival times of the received signals from file T0331D : number of waveforms vs. arrival time (see parameter descriptions in Table 4). . . . . 55

80. Sample waveforms of the received signals after alignment from file T0331E (see parameter descriptions in Table 4) . . . . . 56

81. Mean received signal from file T0331E (see parameter descriptions in Table 4). . . . . 56

82. Standard deviation of the received signals from file T0331E (see parameter descriptions in Table 4) . . . . . 57

83. Signal-to-noise ratio of the received signals from file T0331E (see parameter descriptions in Table 4) . . . . . 57

84. History of the arrival times of the received signals from file T0331E (see parameter descriptions in Table 4). . . . . 58

85. Histogram of the arrival times of the received signals from file T0331E : number of waveforms vs. arrival time (see parameter descriptions in Table 4). . . . . 58

# LIST OF TABLES


| Table | | Page |
|---|---|---|
| 1. | Laser specifications | 11 |
| 2. | Optical system specifications | 11 |
| 3. | Receiver electronics | 12 |
| 4. | List of horizontal path experiments conducted at NASA-GSFC during the last week of March, 1983 | 19 |

# 1. INTRODUCTION

The technique of using atmospheric dispersion to estimate atmospheric delay was first proposed by Bender and Owens[1] in 1965. Since then, many researchers have used this technique for applications in global surveying, geophysical research, and positioning.[2,3,4] More recently, there has been considerable interest in developing remote sensing techniques for the global measurements of temperature and pressure based on the theory of atmospheric dispersion. Gardner[5] has proposed a pressure measurement technique which uses a pulsed two-color laser altimeter for ranging over the ocean. The success of this technique depends on the accuracy in measuring the differential propagation time. In general, picosecond accuracy in differential arrival-time measurement is required in order to achieve millibar-level pressure measurements. In a recent paper, we have expanded the theory on differential arrival-time estimation to include speckle noise.[6] To demonstrate the feasibility of this technique, Abshire et al.[7,8] have conducted preliminary experimental studies by ranging to retro-reflectors over horizontal paths. The experimental timing accuracy was about 6 picoseconds. This corresponds to a pressure measurement accuracy of 3 millibars at nadir. In this report, we describe recent pulsed measurements of atmospheric delay obtained by ranging to the more realistic targets including a simulated-ocean target and an extended plate target. These measurements are used to estimate the expected timing accuracy of a correlation receiver system. The experimental work reported here was conducted using a pulsed two-color laser altimeter developed at NASA-GSFC.

## 2. TARGET CONFIGURATIONS

Abshire et al.[7,8] have done extensive experimental studies on the differential arrival time and the atmospheric delay of optical returns by ranging to retro-reflectors over the horizontal paths using the 355- and 1064-nm wavelengths. They have also performed experiments on single-color returns from an adjustable extended target over the horizontal paths to test various receiver processing algorithms as well as to identify error sources.[8] The experiment involved a "V"-shaped target which consisted of 14 plastic bicycle reflectors on adjustable mounts to simulate the depth-distributed specular returns from the ocean surface. The test results indicated that it is possible to resolve the returns from individual bicycle reflectors. The fluctuation of the strengths between shots in the return was believed to be caused by the combination of shot noise and speckle-induced fluctuations introduced by the target.

In an attempt to identify the different noise sources, we conducted additional experiments in March, 1983. The main objectives of these new experiments were to further study the speckle-noise effect on the received pulses and to investigate the timing performance of a correlation receiver based on the measurements which we obtained for the various target configurations. In this chapter, the detailed descriptions of the ranging path and the target configurations are furnished.

The experiment took place at NASA-GSFC during the last week of March, 1983. During the experiment, the laser pulses were transmitted over a horizontal path using a periscope mirror (Fig. 1) mounted permanently on the

roof of the laboratory. The ranging targets were located on the roof of another building at approximately the same altitude. The round-trip distance between the targets and the ranging system was 753 m.

The first target that was used in the experiment was a 36" by 1.5" flat plate covered by reflective tape. A single retro-reflector was mounted 9" in front of the plate. It was used for comparison and alignment purposes. The front view of this target is shown in Fig. 2. It should be noted that the radius of the laser footprint was on the order of one centimeter. Since the length of the plate target was 36", the amount of pulse broadening could be controlled by tilting the target surface at the appropriate angle. This configuration is a typical example of a continuous range-spread target. The amount of range spread (S) is given by

$$S = L \cos\phi \ , \qquad (1)$$

where L is the length of the plate target, and $\phi$ is the tilting angle between the plate target and the ray of incidence.

After a few sets of raw data for this target configuration were collected, we discovered that some of the received pulses on each data set contained only minimal energy from both the retro-reflector and the plate target. We later concluded that the plate target of 1.5" width was simply too narrow to compensate for the effect of vertical laser beam wandering. During some measurements, the turbulence steered the beam off target, which accounted for the small return energy. In order to correct this problem, a

36" by 6" flat plate was used to replace the old target. The new target is shown in Fig. 3.

The return pulses from these targets have widths of about twice the amount of range spread. Since each received pulse width is longer than the speckle correlation length, the target-induced speckle causes random small-scale fluctuation within an individual received pulse.[9]

The second target was a simplified version of the "V"-shaped, extended target in Abshire's experiment. In this configuration, one side of the "V" was covered by the non-reflective blanket so that the target became an array of seven bicycle reflectors with each reflector offset by 6" behind and 1" to the right of the previous reflector. Each individual reflector had a 2.5" dia. circular reflecting surface which consisted of a plastic shield on top of the numerous small cube-corner reflectors. Since the plastic shield had an optically rough surface, much of the reflected energy was scattered away from the receiving telescope so that the back-scattered signal was more difficult to detect. To overcome this difficulty, a retro-reflector was placed 9" in front of the first bicycle reflector. With this strong returned signal from the retro-reflector as a reference, it was relatively easy to locate the target return. The picture of this target is shown in Fig. 4.

In this configuration, the target array as a whole is a range-spread target, but each bicycle reflector consists of numerous non-dispersive cube-corner reflectors. As a result, the target-induced speckle will cause random fluctuations in the total received energy as well as small-scale fluctuation within each received pulse.

ORIGINAL PAGE IS
OF POOR QUALITY

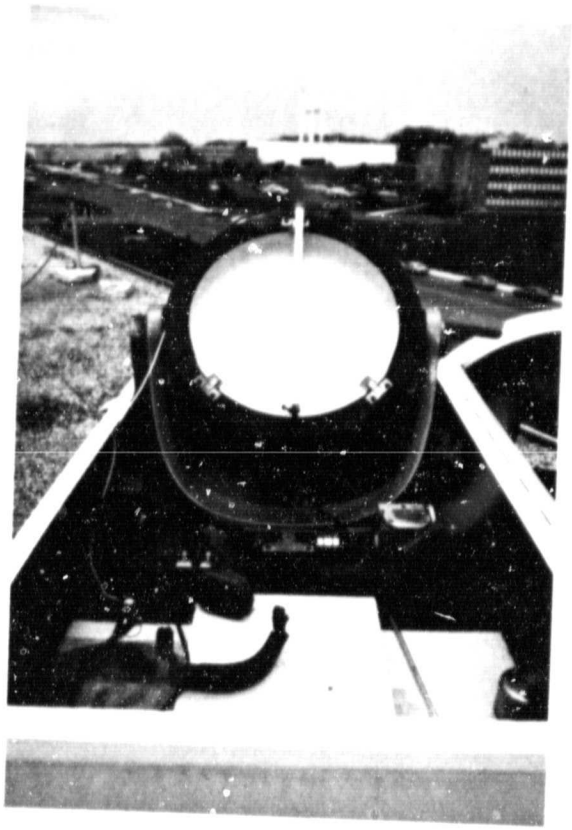

Figure 1. Front view of the periscope mirror.

ORIGINAL PAGE IS
OF POOR QUALITY

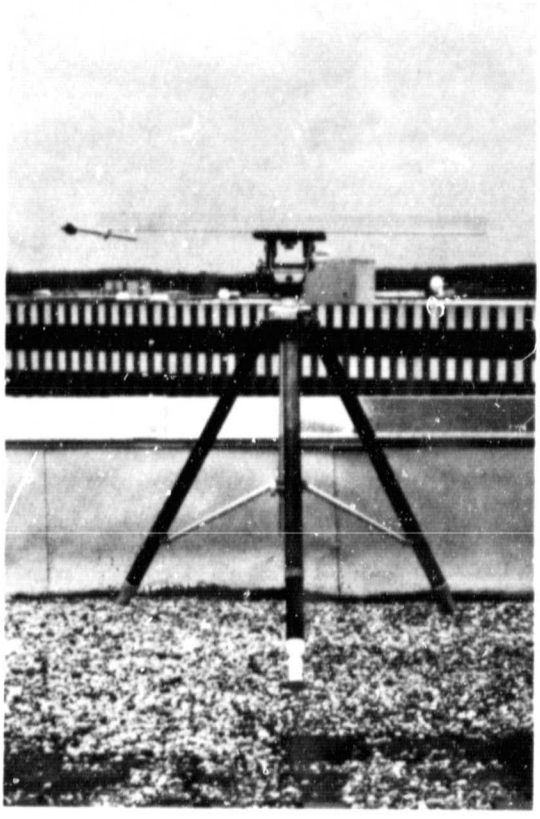

Figure 2. Front view of the 36" by 1.5" flat plate target and reference retroreflector.

ORIGINAL PAGE IS
OF POOR QUALITY

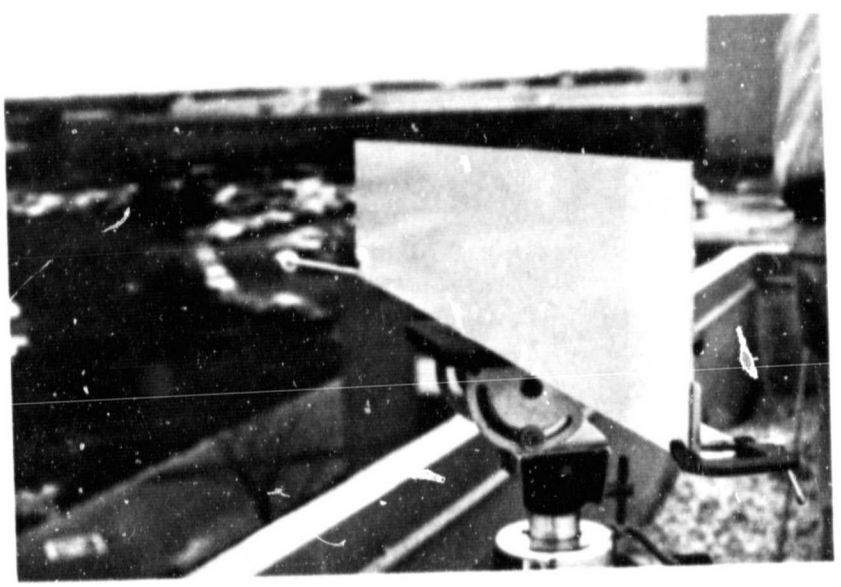

Figure 3. Side view of the 36" by 6" flat plate target and reference retroreflector.

ORIGINAL PAGE IS
OF POOR QUALITY

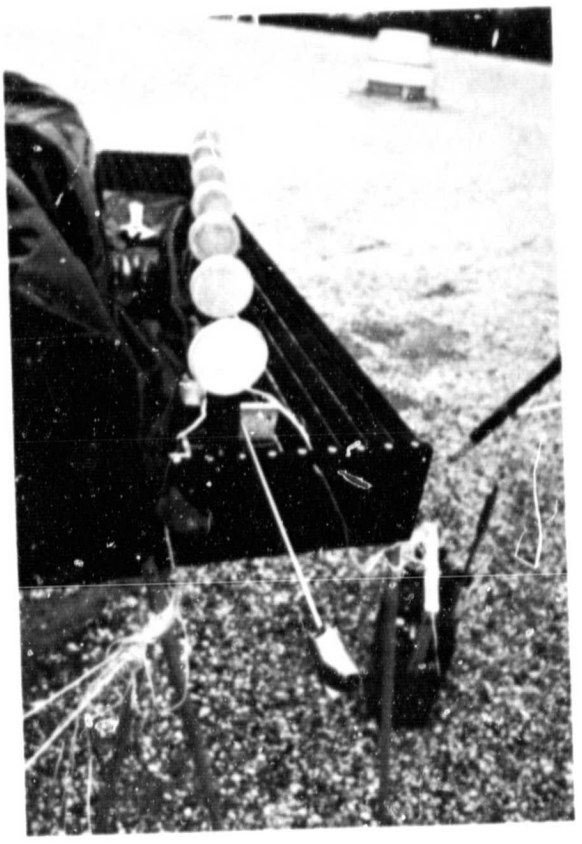

Figure 4. Front view of the bicycle reflector array and reference retroreflector.

# 3. SYSTEM HARDWARE

A pulsed laser ranging system was constructed and developed at NASA-GSFC for the experimental two-color laser altimetry research. The objectives for building this system were both to verify the theoretical instrument performance and to determine the technical limits in measuring the atmospheric delay. This system has gone through many modifications in order to improve its performance. The block diagram of an older version of this system is shown in Fig. 5, and summaries of the norminal specifications of the laser, optical, and receiver subsystems are given in Tables 1, 2, and 3, respectively. In the new ranging system that we used throughout our experiments, the bias error in measuring the atmospheric delay was reduced by using a single detector for both the 355- and 1064-nm pulses and by reducing the magnification in the receiver optics. Both of these changes have been incorporated into the receiver design shown in Fig. 6. This subsystem has replaced the subsystem within the dashed lines in Fig. 5. Airborne experiments using this system are also planned for measurements over the ocean later this year. In the future, a dual-channel streak tube camera-based receiver system will be employed to replace the waveform digitizer which will yield a much higher time resolution. This chapter outlines the operation of the ranging system for the horizontal path experiment. Detailed descriptions of the subsystems and their performance limitations can be found in [7].

During the experiment, the mode-locked frequency-tripled ND:YAG laser transmitter produced optical pulses at 1064 nm. A small fraction (about 4%)

ORIGINAL PAGE IS
OF POOR QUALITY

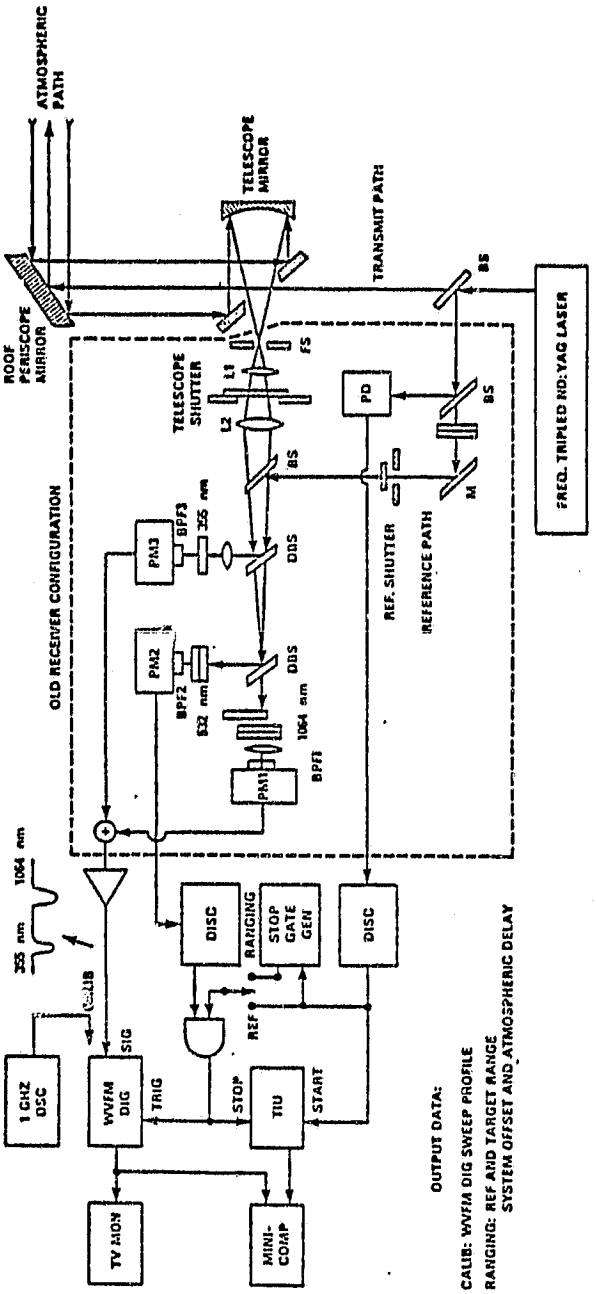


Figure 5. The laser ranging system with the old receiver configuration.

| | |
|---|---|
| Manufacturer: | Quantel International, Model YG40 |
| Dye type: | Kodak Q-Switch-1 A9740 |
| Laser rods: | ND:YAG, 6 mm diameter, 65 mm long |
| Harmonic conversion crystals: | KD*P - Type 1 |
| Output energy: | 6 mJ at 1064 nm, 3 mJ at 532 nm, 1 mJ at 355 nm |
| Output pulse width: | 60 - 100 psec (nominal) |
| Repetition rate: | 5 pulses per second |

Table 1. Laser specifications

| | | |
|---|---|---|
| Turning mirrors: | | Enhanced Al surface |
| Roof mirror: | | 38 cm dia. flat, enhanced Al surface |
| Telescope assembly: | | Elliptical cross-section, 459 sq. cm collection area, 91.4 cm focal length |
| Field stop: | | 0.16 cm dia., telescope FOV = 1.78 mrad |
| Narrow-band filters: | | 355 nm: 10 nm FWHM, 532 nm: 2 nm FWHM, 1064 nm: 2 nm FWHM |
| Photomultipliers: | | Varian 154 static-crossed-field, 160 psec impulse response |
| | PM3: | S-20 photocathode, QE 17% at 355 nm |
| | PM2: | InGaAsP photocathode, QE 12% at 532 nm |
| | PM1: | InGaAsP photocathode, QE 2.8% at 1064 nm mounted in housing at approx. -10 deg. C |

Table 2. Optical system specifications

| | |
|---|---|
| Calibration source: | 1 GHz VCO, manually tuned and referenced to frequency counter |
| Discriminators: | Ortec 934, constant fraction type |
| Time interval unit: | Hewlett-Packard 5370, 100 psec accuracy |
| Stop gate generator: | Ortec 416A Gate and Delay generator |
| Waveform digitizer: | Tektronix R7912 with 7A29 and 7B15 plug-ins, 600 MHz bandwidth, 500 psec/div sweep speed |
| Minicomputer: | Digital Equipment Corporation Minc-11, with LSI 11/23 processor, RT-11 operating system |

Table 3. Receiver Electronics

ORIGINAL PAGE IS
OF POOR QUALITY



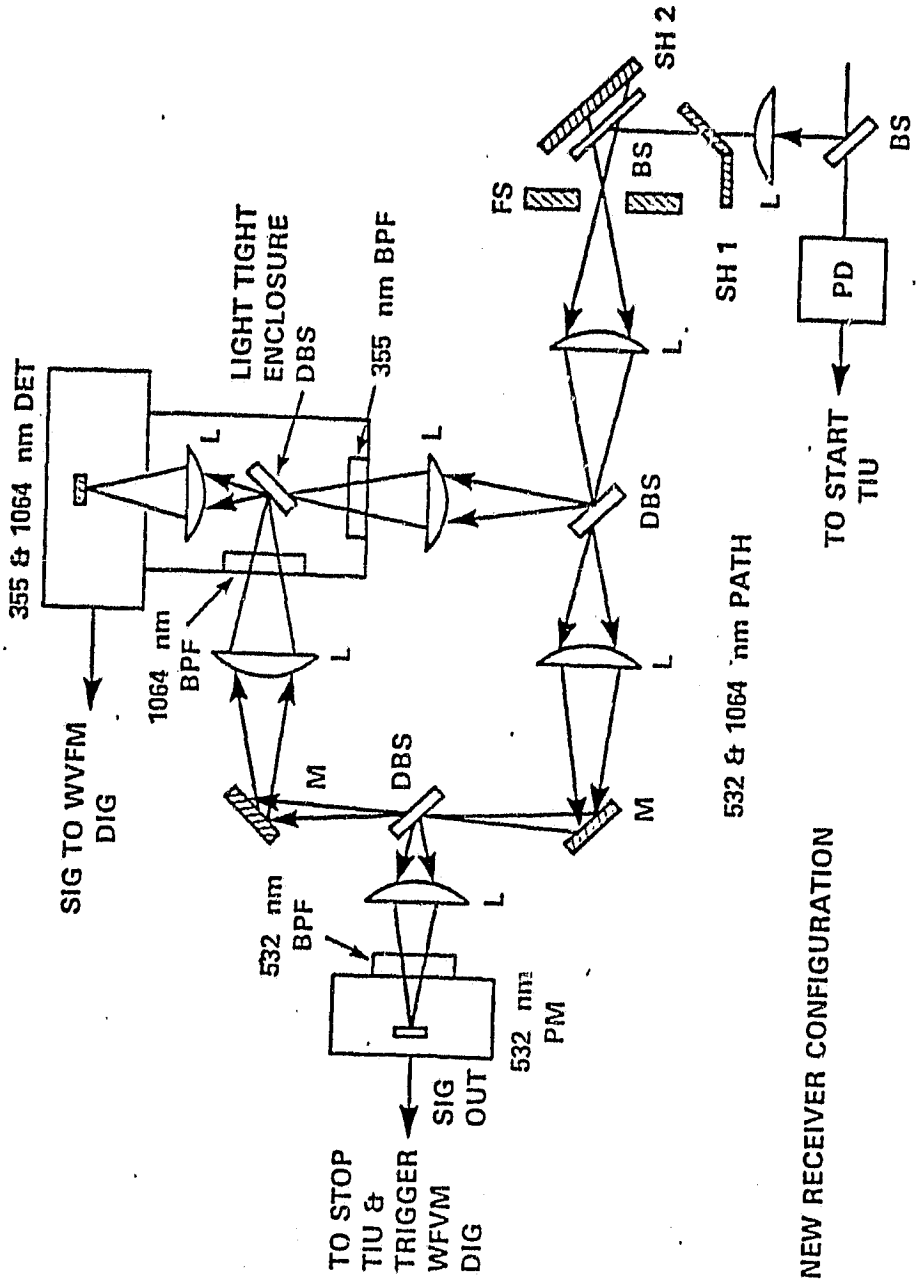


Figure 6. New receiver configuration.

of the transmitted energy was reflected by a beam splitter into the reference path to trigger the timing circuit. The remainder of the energy passed through a beam splitter and was directed over the atmospheric path to the target reflector(s). The reflected energy was collected by the telescope and was directed through a shutter into the receiver assembly. The amount of collected energy was varied from one set of data to the next by carefully controlling the effective collection area of the receiver telescope.

This system was operated in the ranging mode to measure the system delays and the atmospheric delay. The photomultiplier outputs were recorded by the Tektronix R7912 waveform digitizer. In these measurements, the time biases caused by digitizer sweep speed nonlinearities and time-walk were minimized by using specially developed calibration procedures. Normally, 200 individual measurements were recorded in this mode. The mean pulse separation time between the returns from the retro-reflector and the target and the mean flight-time reading were then computed from these data.

The waveforms of the received pulses are of principal interest in this experiment because of their applications to remote pressure measurements. In the following chapters, the detailed description of the waveform processing and the analysis of the timing performance of a correlation receiver using these waveforms are given.

## 4. DATA PROCESSING

Several sets of returned pulses from both the plate target and the bicycle reflector array were collected. Different data sets of the same target configuration correspond to measurements taken with different receiving aperture sizes and/or at different times.

There are 200 individual waveforms of the received signals recorded in each data set. Due to the photomultiplier and digitizer time jitter, the waveforms appear to shift temporally from pulse to pulse in a random fashion. This time jitter would contribute additional error to the timing accuracy of the receiver if left uncorrected. Since we are only interested in the differential arrival time between the retro-reflector returns and the target returns, we can correct the time-jitter problems by using the peak returns from the retro-reflector as the time reference. Specifically, the time positions of the retro-reflector peak returns are first determined by using a center-of-mass algorithm. A mean peak position is then computed, and all the waveforms are aligned with respect to this mean peak position. After the waveforms in a data set are aligned, the corresponding mean, standard deviation, and the signal-to-noise ratio for that set of data are computed.

If an individual received signal is denoted by $S(t)$, and the mean received signal by $\bar{S}(t)$, then the correlation receiver estimates the arrival time according to

$$\hat{\tau}_c = \arg \max_{\tau} \{ \int_{-\infty}^{\infty} dt \; S(t) \; \bar{S}(t + \tau) \} \; . \qquad (2)$$

In this experiment, the arrival times of the returned pulses from the plate and the bicycle reflector targets are the principal interests. Because each aligned waveform in every data set also includes the retro-reflector return of 1000 psec FWHM width which contaminates a portion of the extended target return, it is necessary to eliminate the retro-reflector returns from the waveforms before correlating. This problem of cross-over is particularly severe in the bicycle reflector returns where the separation times between the peak retro-reflector returns and the peak returns from the first bicycle reflector are only about 750 psec. In order to recover the net extended target returns, the first halves of the retro-reflector returns and their mirror images are subtracted from the return waveforms. A typical return waveform which included both the returns from the bicycle reflectors and the retro-reflector is shown in Fig. 7(a), and the same waveform after subtracting the retro-reflector return is shown in Fig. 7(b). We can see that the tail of the return from the first bicycle reflector is recovered very nicely. The pulse subtraction routine has been incorporated into the correlation algorithm. The first part of this algorithm finds the mirror image and performs the subtraction. The second part performs the correlation between the resultant mean waveform of the data and each individual resultant waveform, and locates the peak of the correlation function. This peak corresponds to the estimate of the time of arrival. The last part of the algorithm calculates the mean and the standard deviation of the arrival time. The results obtained using this algorithm are then presented in the forms of a history plot and a histogram.

The results are shown in Fig. 8 through Fig. 85. A list of different

ORIGINAL PAGE IS
OF POOR QUALITY



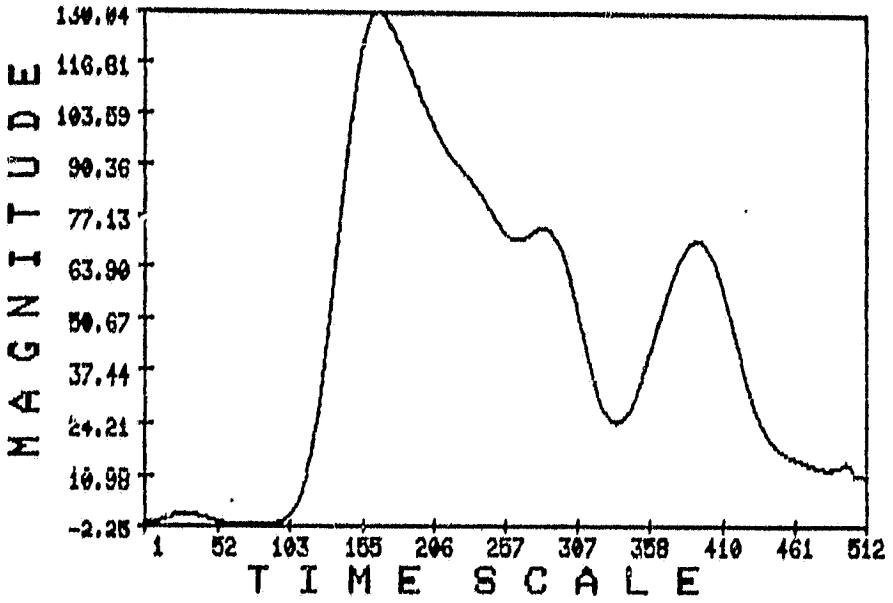


Figure 7(a). A typical return waveform which contains both the returns from the bicycle reflector array and the retro-reflector.

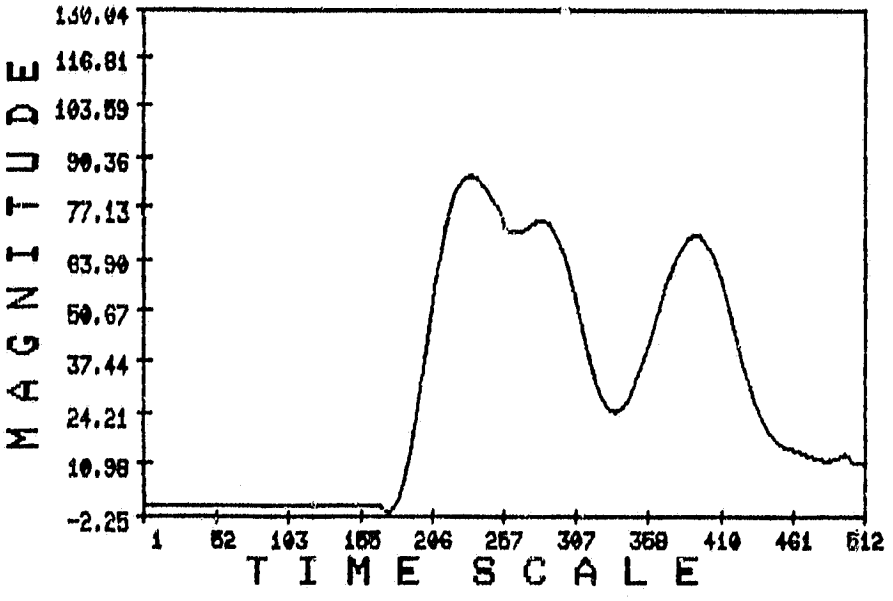


Figure 7(b). The same waveform after subtracting the retro-reflector return.

target configurations and parameters associated with these results is given in Table 4.

ORIGINAL PAGE IS
OF POOR QUALITY



| File Name | Target Configuration | Tilt. Angle (deg) | Rec. Apert. (sq.cm) | Laser Pulse Width (psec) | Time Scale (ps/unit) | Mag. Scale (pe/unit) |
|---|---|---|---|---|---|---|
| P0329A | 36"x1.5" Plate | 45 | 459 | 60 | 19.53 | 0.142 |
| P0329B | 36"x1.5" Plate | 45 | 301 | 60 | 19.53 | 0.142 |
| P0329C | 36"x1.5" Plate | 45 | 172 | 60 | 19.53 | 0.142 |
| P0401A | 36"x6" Plate | 30 | 459 | 100 | 19.53 | 0.568 |
| P0401B | 36"x6" Plate | 30 | 301 | 100 | 19.53 | 0.568 |
| P0401C | 36"x6" Plate | 30 | 172 | 100 | 19.53 | 0.568 |
| P0401D | 36"x6" Plate | 30 | 71 | 100 | 19.53 | 0.284 |
| P0401E | 36"x6" Plate | 30 | 32 | 100 | 19.53 | 0.0568 |
| T0331A | Bike Reflectors | | 459 | 100 | 19.53 | 1.42 |
| T0331B | Bike Reflectors | | 301 | 100 | 19.53 | 1.42 |
| T0331C | Bike Reflectors | | 172 | 100 | 19.53 | 1.42 |
| T0331D | Bike Reflectors | | 71 | 100 | 19.53 | 1.42 |
| T0331E | Bike Reflectors | | 32 | 100 | 19.53 | 1.42 |

Table 4. List of horizontal path experiments conducted at NASA-GSFC during the last week of March, 1983.

**Note: 1. The time scale applies to all the plots, the timing histories, and the timing histograms.
2. The magnitude scale applies only to the waveforms of the received signals and the mean signals, and the standard deviation plots.

ORIGINAL PAGE IS
OF POOR QUALITY



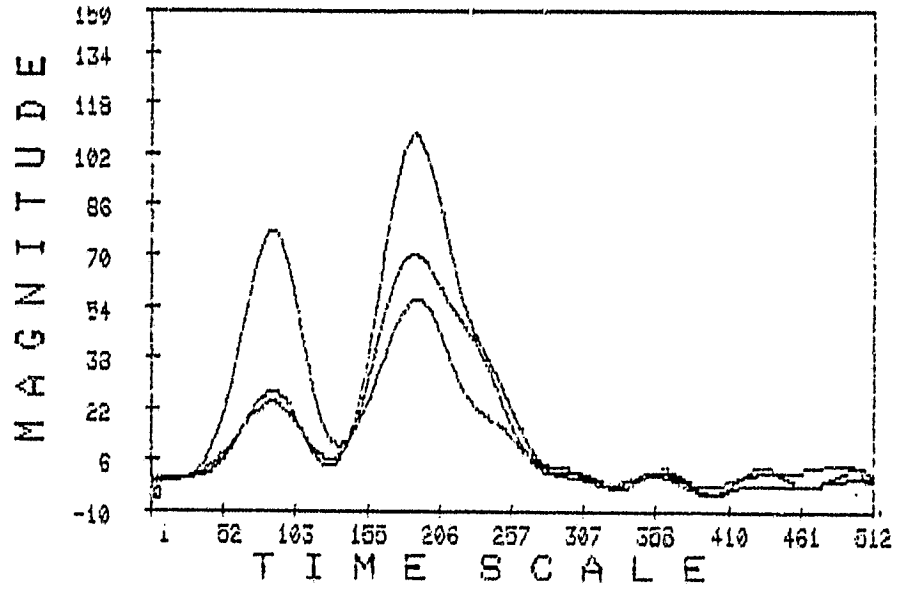


Figure 8. Sample waveforms of the received signals after alignment from file P0329A (see parameter descriptions in Table 4).

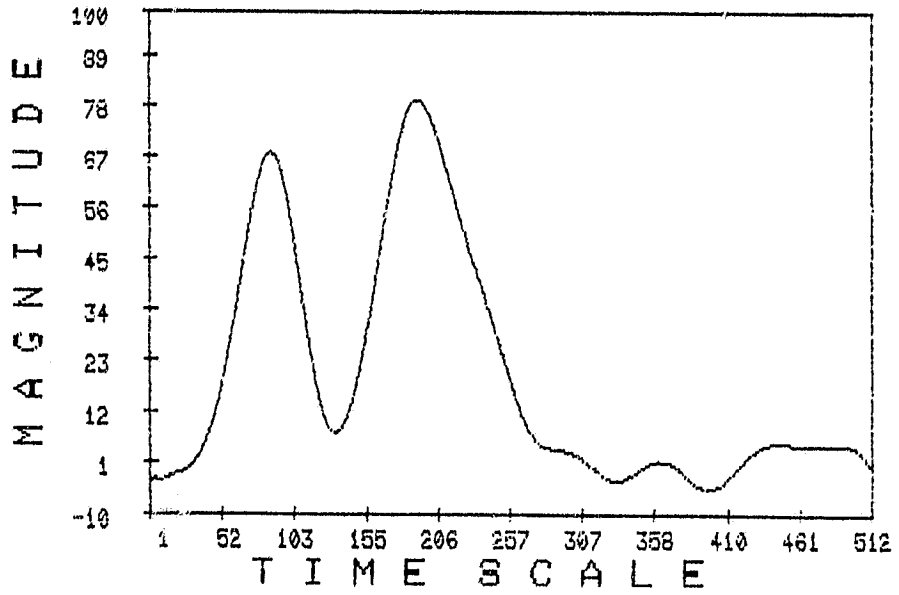


Figure 9. Mean received signal from file P0329A (see parameter descriptions in Table 4).

ORIGINAL PAGE IS
OF POOR QUALITY



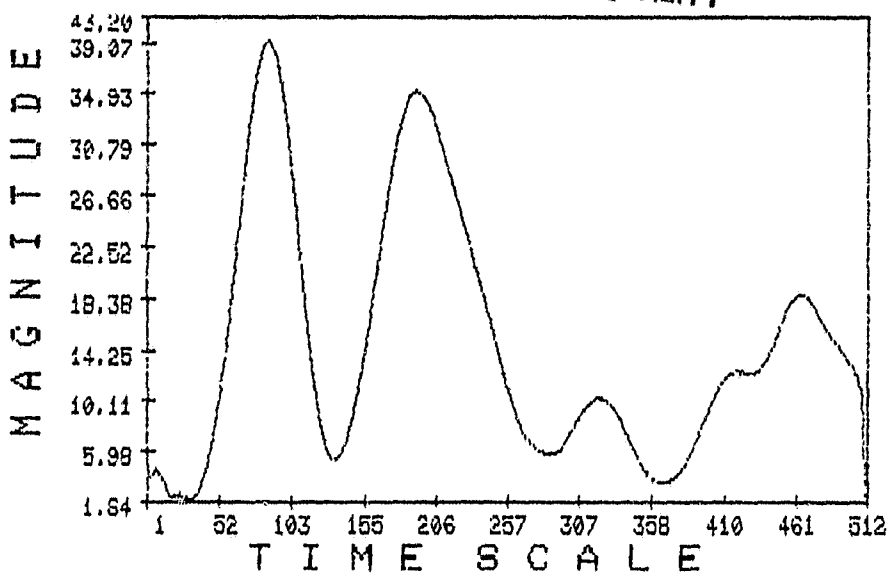


Figure 10. Standard deviation of the received signals from file P0329A (see parameter descriptions in Table 4).

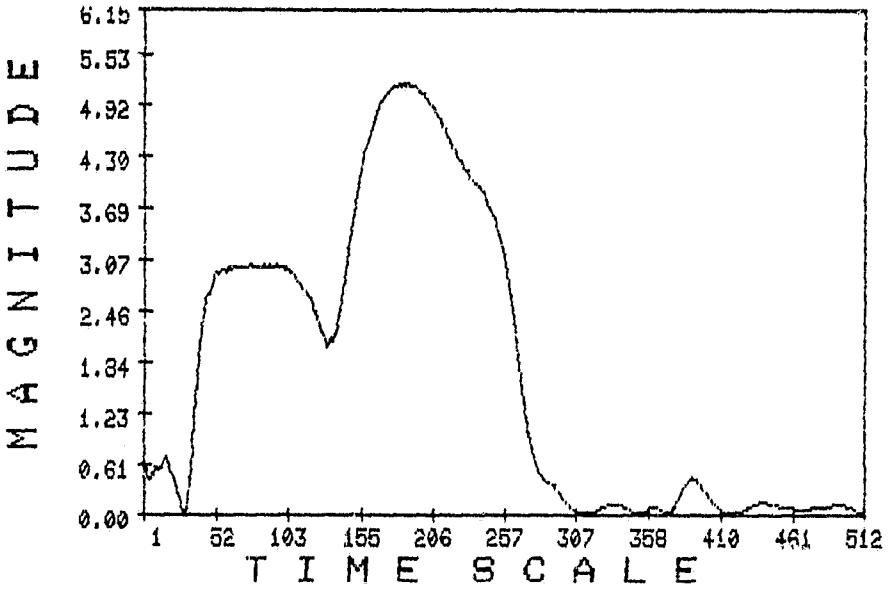


Figure 11. Signal-to-noise ratio of the received signals from file P0329A (see parameter descriptions in Table 4).

ORIGINAL PAGE IS
OF POOR QUALITY



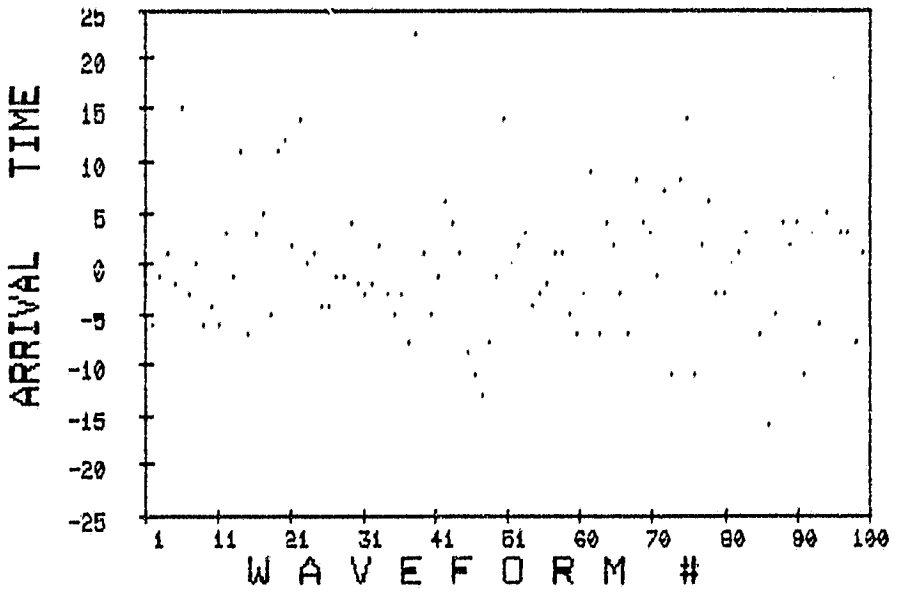


Figure 12. History of the arrival times of the received signals from file P0329A (see parameter descriptions in Table 4).

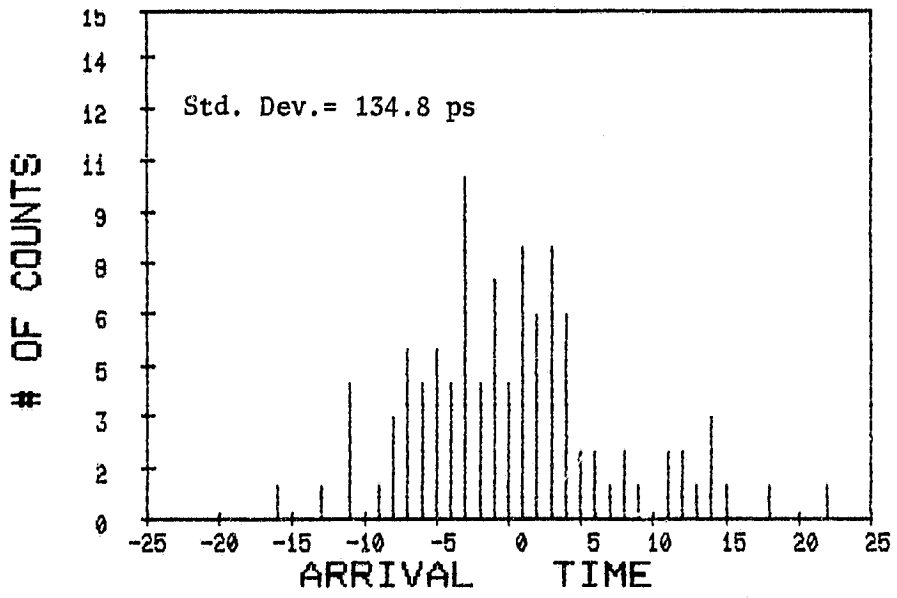


Figure 13. Histogram of the arrival times of the received signals from file P0329A : number of waveforms vs. arrival time (see parameter descriptions in Table 4).

ORIGINAL PAGE IS
OF POOR QUALITY

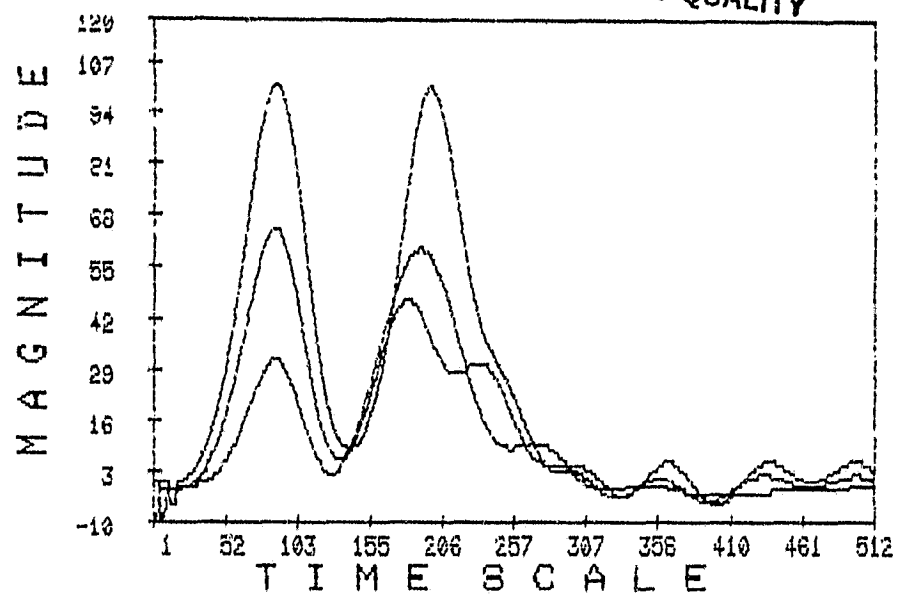


Figure 14. Sample waveforms of the received signals after alignment from file P0329B (see parameter descriptions in Table 4).

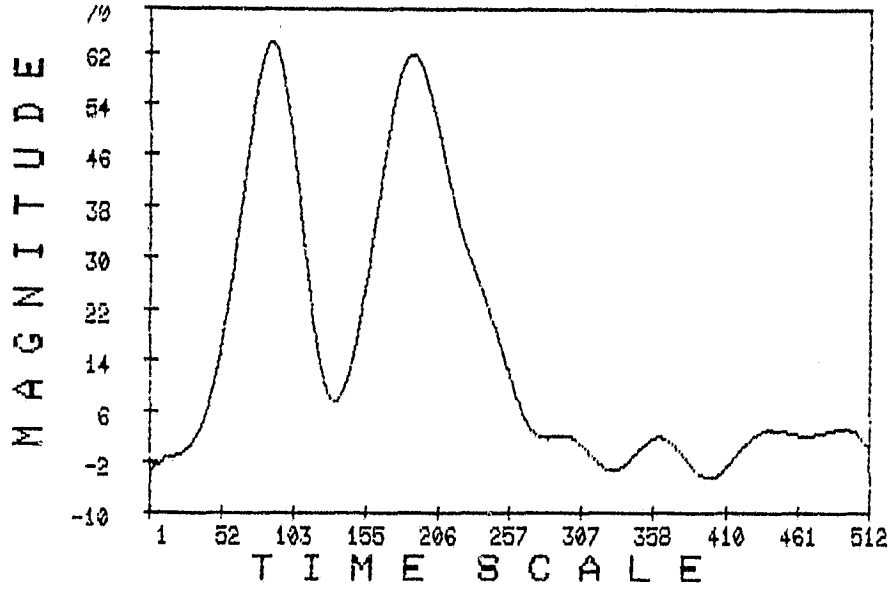


Figure 15. Mean received signal from file P0329B (see parameter descriptions in Table 4).

ORIGINAL PAGE IS
OF POOR QUALITY



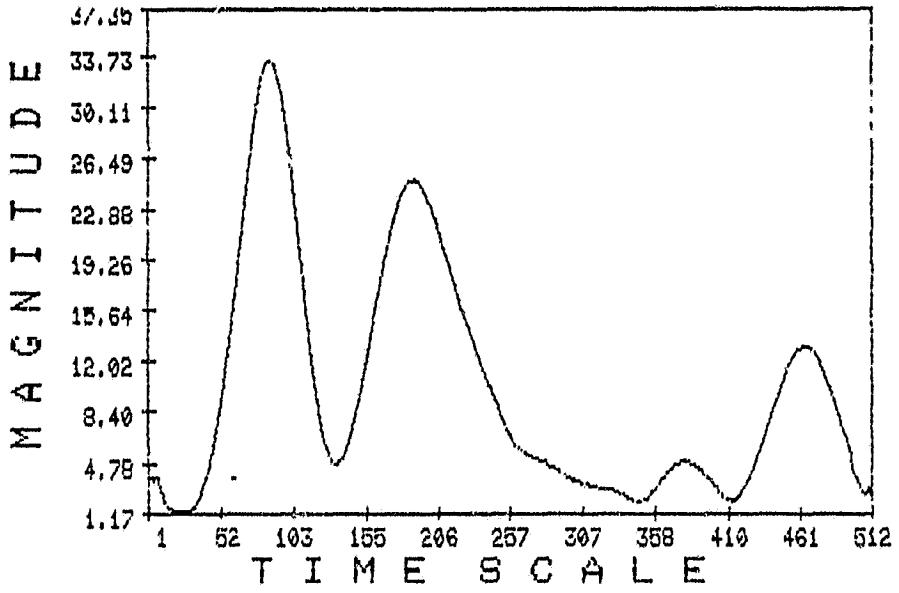


Figure 16. Standard deviation of the received signals from file P0329B (see parameter descriptions in Table 4).

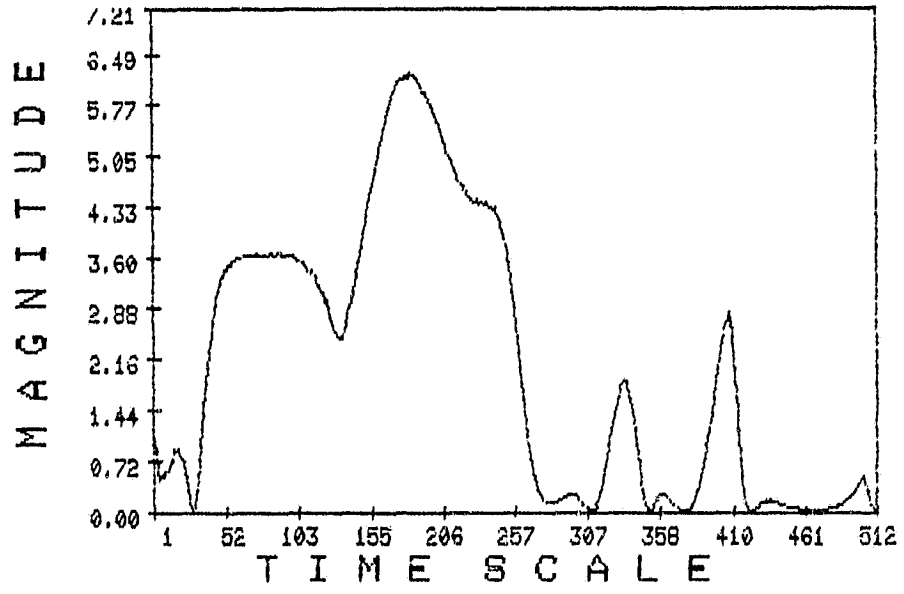


Figure 17. Signal-to-noise ratio of the received signals from file P0329B (see parameter descriptions in Table 4).

ORIGINAL PAGE IS
OF POOR QUALITY



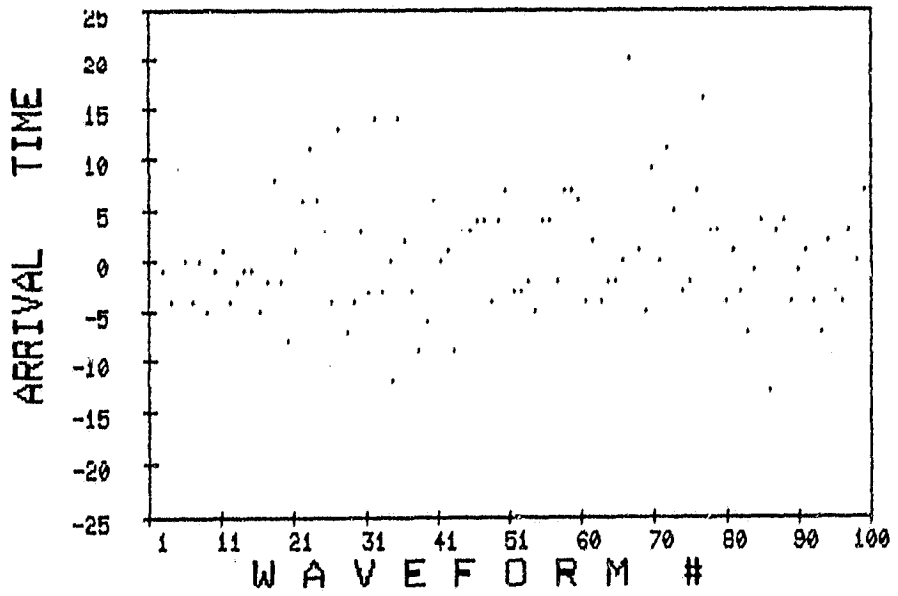


Figure 18. History of the arrival times of the received signals from file P0329B (see parameter descriptions in Table 4).

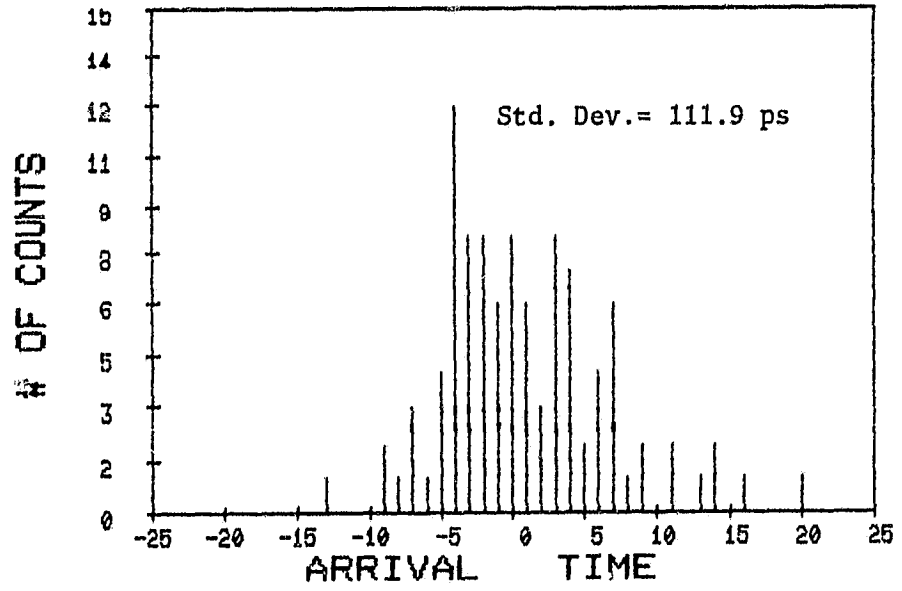


Figure 19. Histogram of the arrival times of the received signals from file P0329B : number of waveforms vs. arrival time (see parameter descriptions in Table 4).

ORIGINAL PAGE IS
OF POOR QUALITY



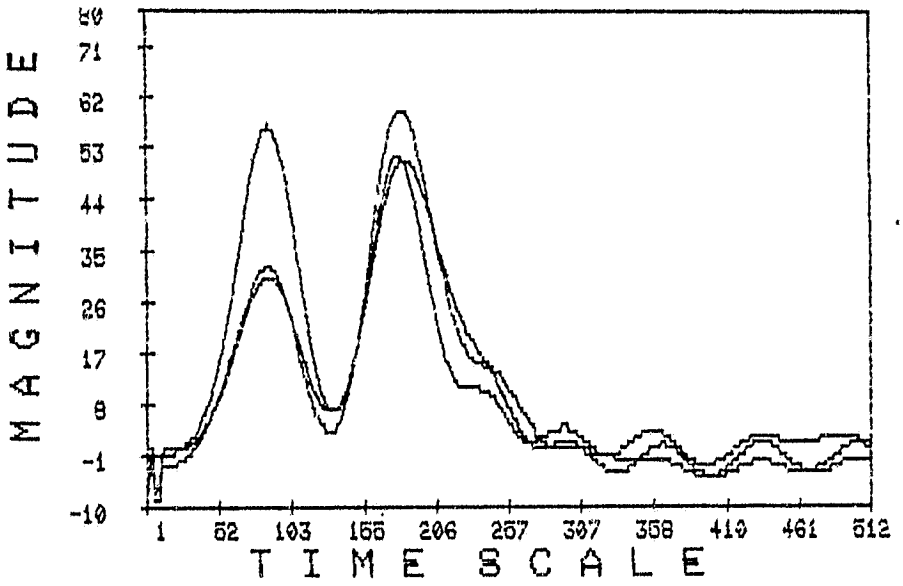


Figure 20. Sample waveforms of the received signals after alignment from file P0329C (see parameter descriptions in Table 4).

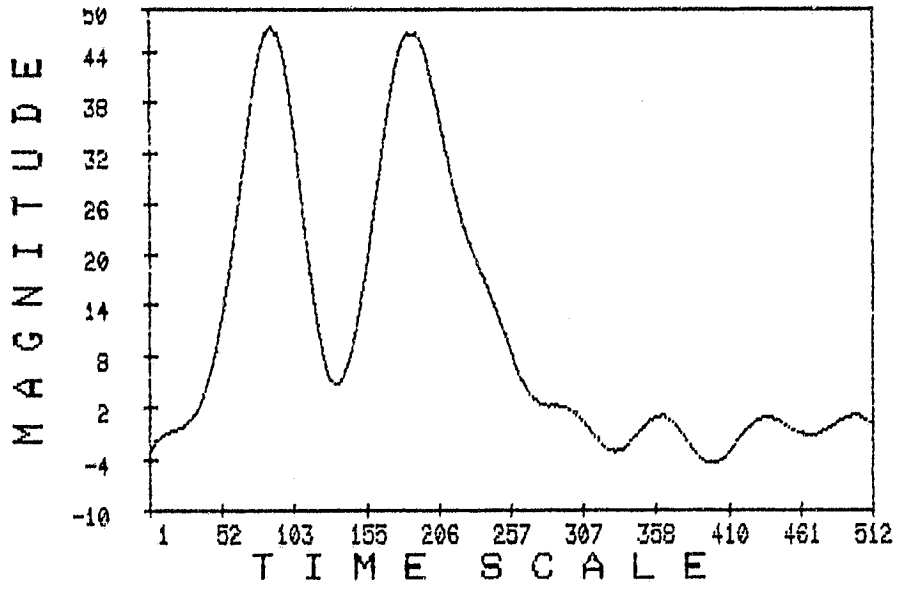


Figure 21. Mean received signal from file P0329C (see parameter descriptions in Table 4).

ORIGINAL PAGE IS
OF POOR QUALITY



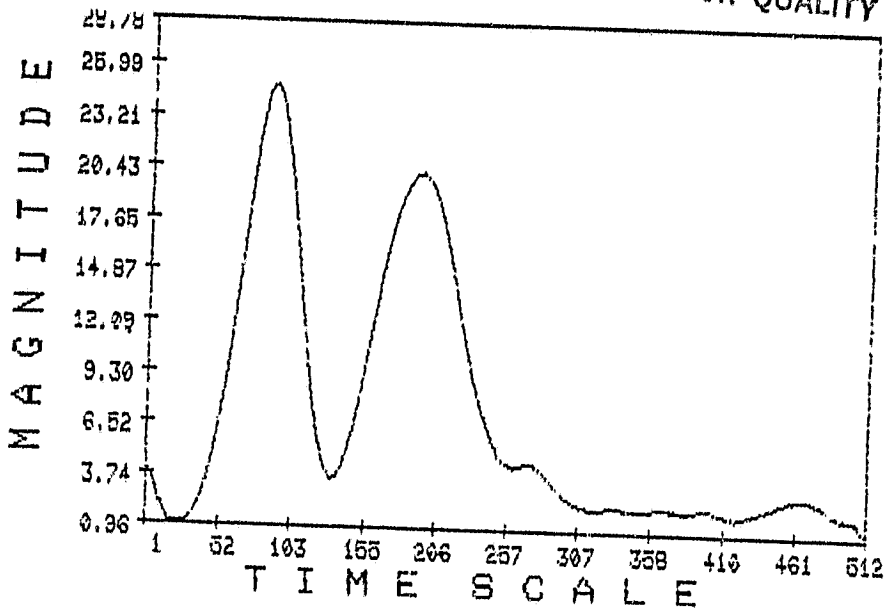


Figure 22. Standard deviation of the received signals from file P0329C (see parameter descriptions in Table 4).

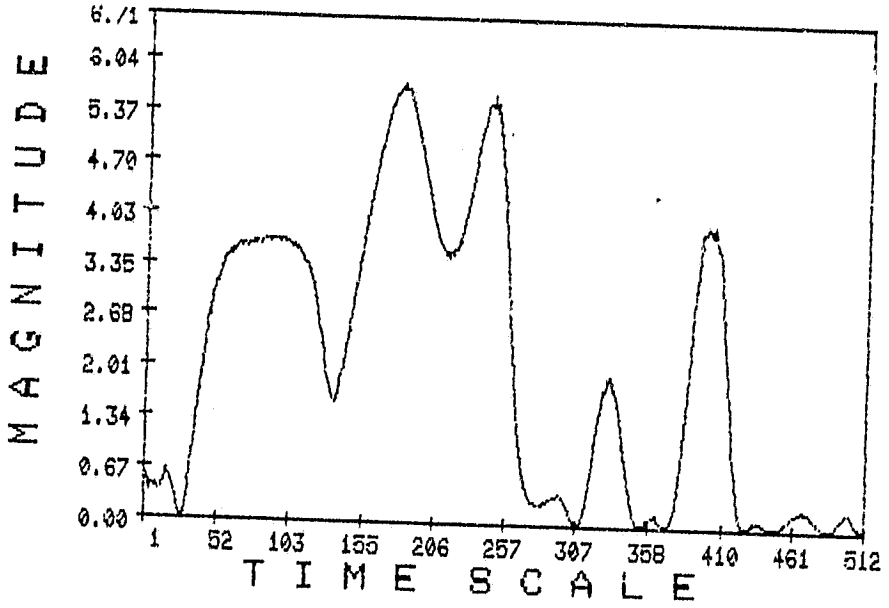


Figure 23. Signal-to-noise ratio of the received signals from file P0329C (see parameter descriptions in Table 4).

ORIGINAL PAGE IS
OF POOR QUALITY



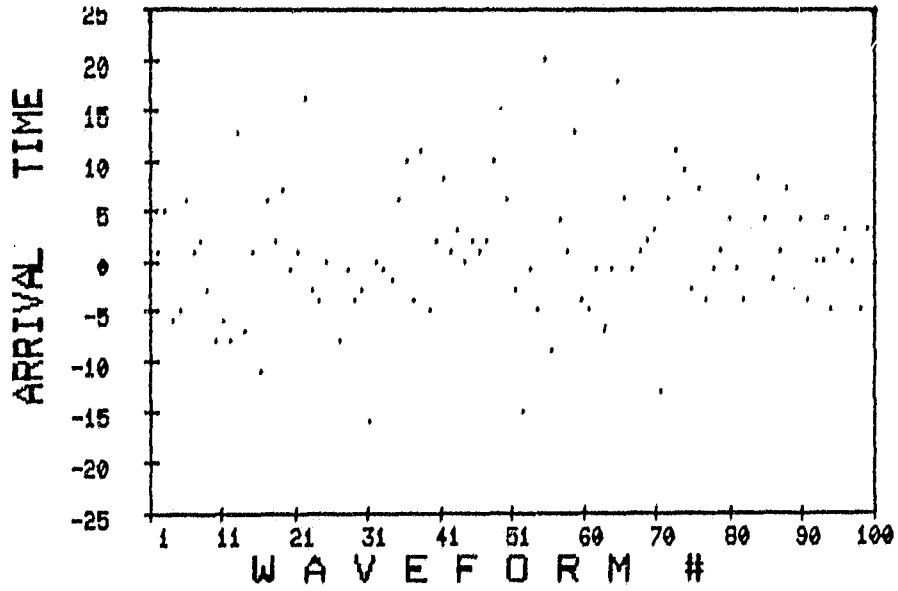


Figure 24. History of the arrival times of the received signals from file P0329C (see parameter descriptions in Table 4).

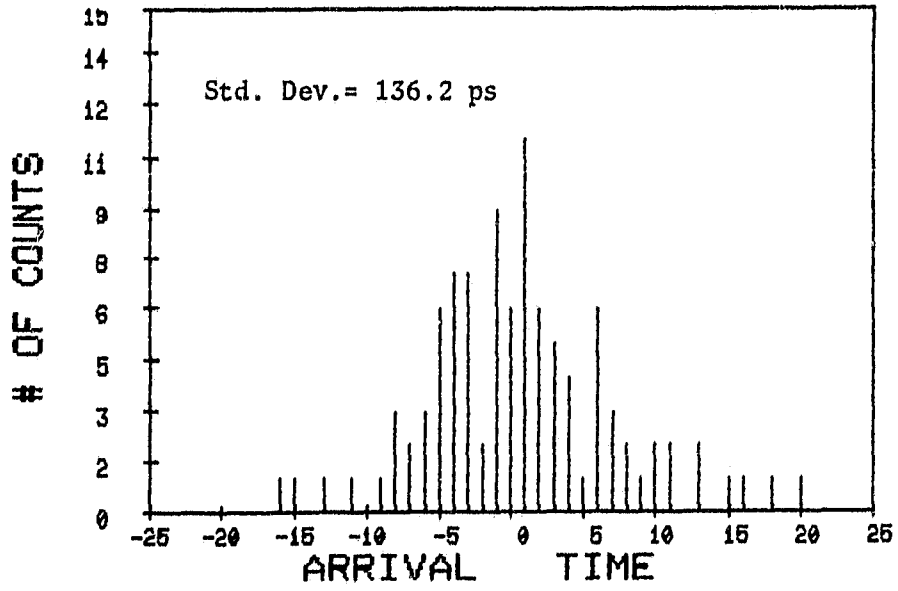


Figure 25. Histogram of the arrival times of the received signals from file P0329C : number of waveforms vs. arrival time (see parameter descriptions in Table 4).

ORIGINAL PAGE IS
OF POOR QUALITY



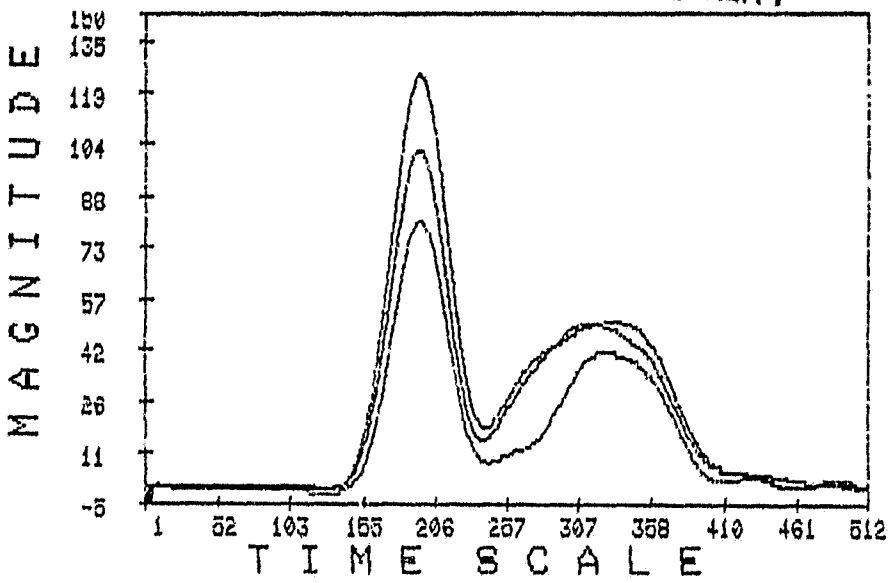


Figure 26. Sample waveforms of the received signals after alignment from file P0401A (see parameter descriptions in Table 4).

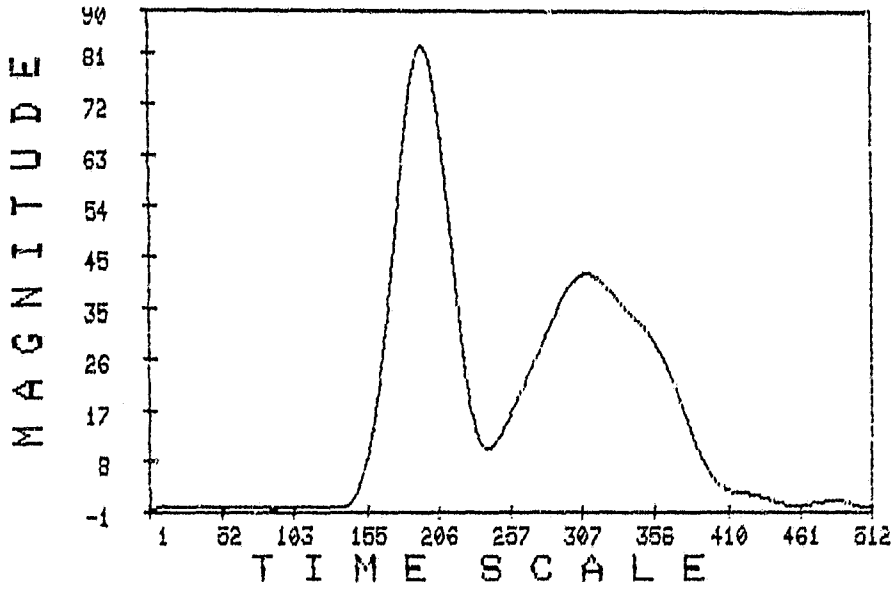


Figure 27. Mean received signal from file P0401A (see parameter descriptions in Table 4).

ORIGINAL PAGE IS
OF POOR QUALITY



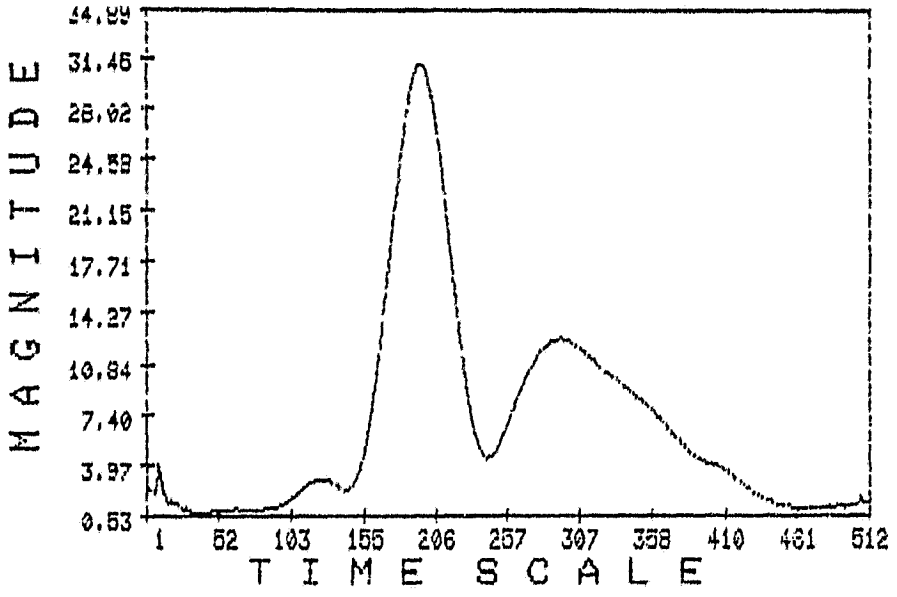


Figure 28. Standard deviation of the received signals from file P0401A (see parameter descriptions in Table 4).

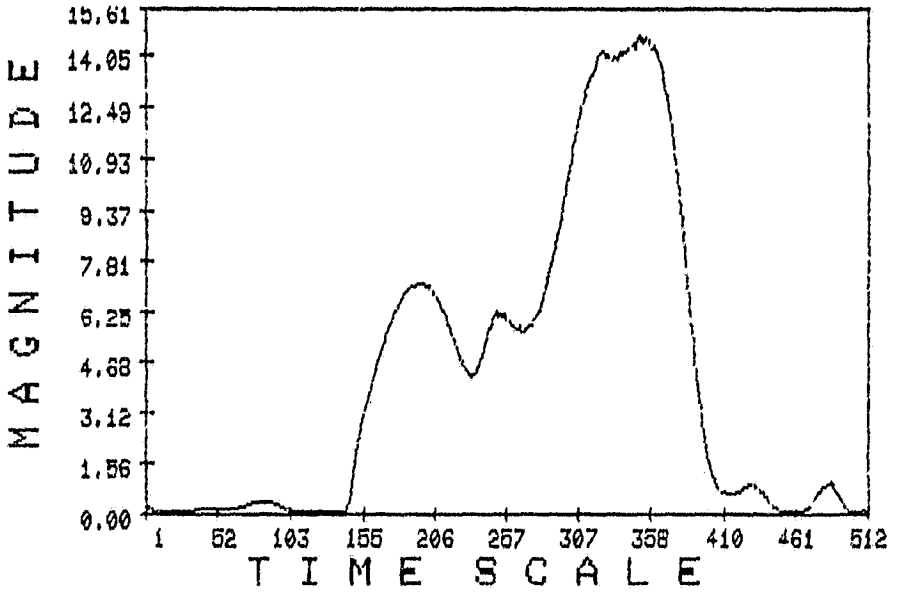


Figure 29. Signal-to-noise ratio of the received signals from file P0401A (see parameter descriptions in Table 4).

ORIGINAL PAGE IS
OF POOR QUALITY



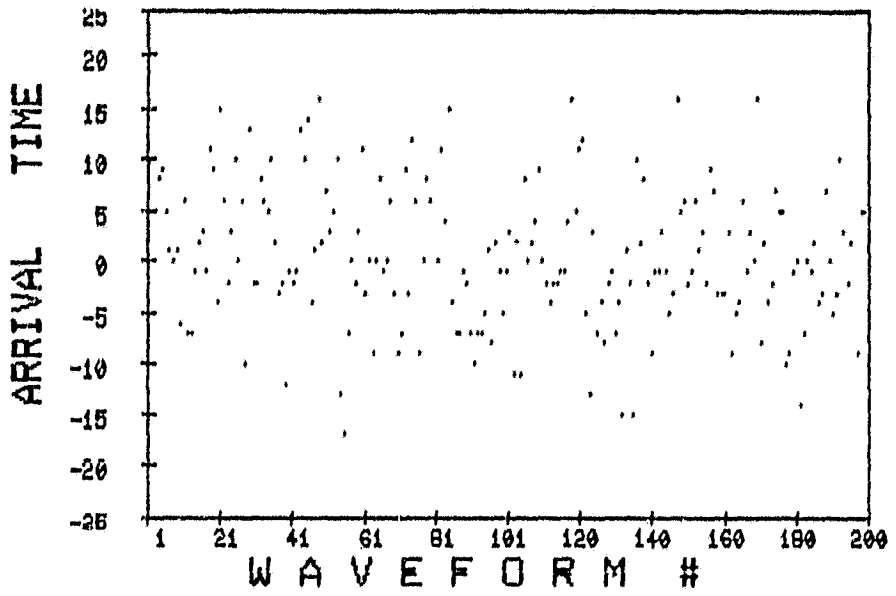


Figure 30. History of the arrival times of the received signals from file P0401A (see parameter descriptions in Table 4).

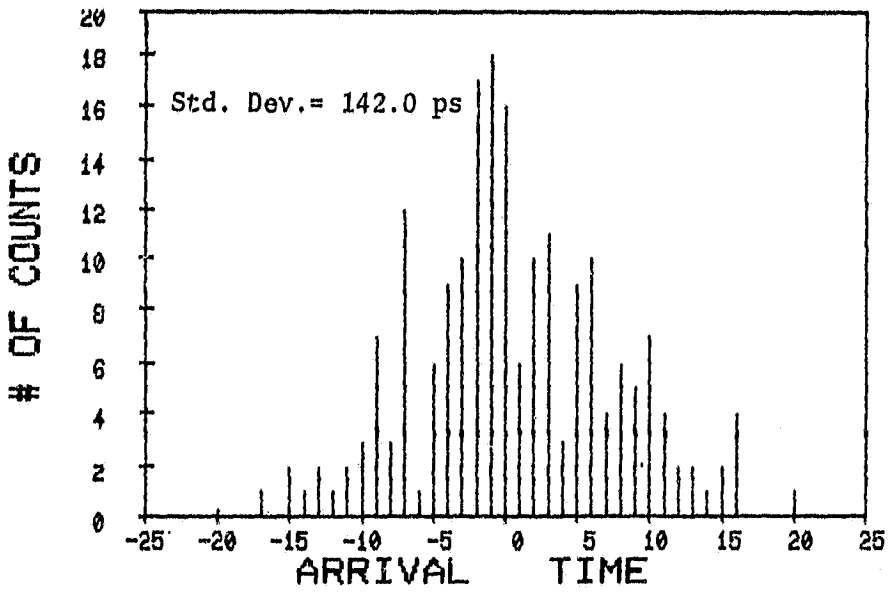


Figure 31. Histogram of the arrival times of the received signals from file P0401A : number of waveforms vs. arrival time (see parameter descriptions in Table 4).

ORIGINAL PAGE IS
OF POOR QUALITY



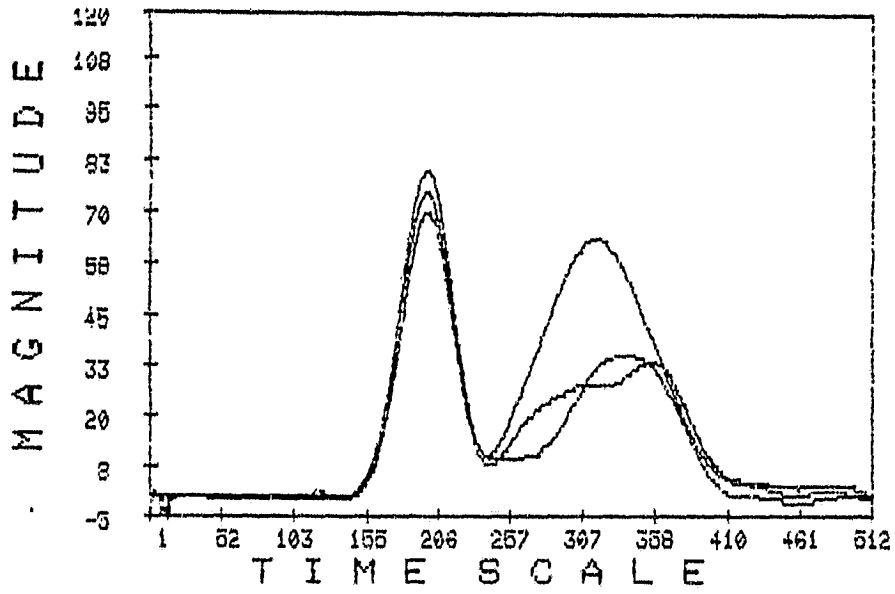


Figure 32. Sample waveforms of the received signals after alignment from file P0401B (see parameter descriptions in Table 4).

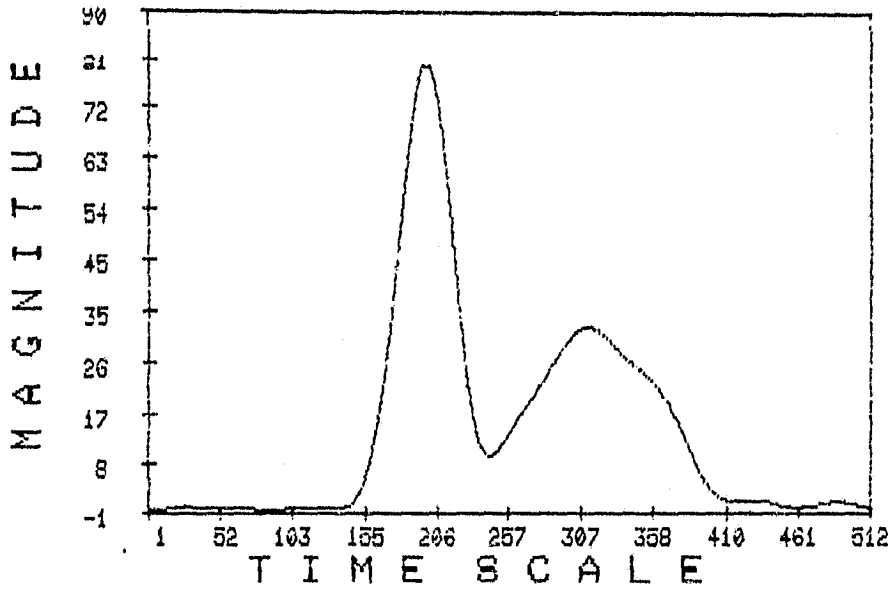


Figure 33. Mean received signal from file P0401B (see parameter descriptions in Table 4).

ORIGINAL PAGE IS
OF POOR QUALITY



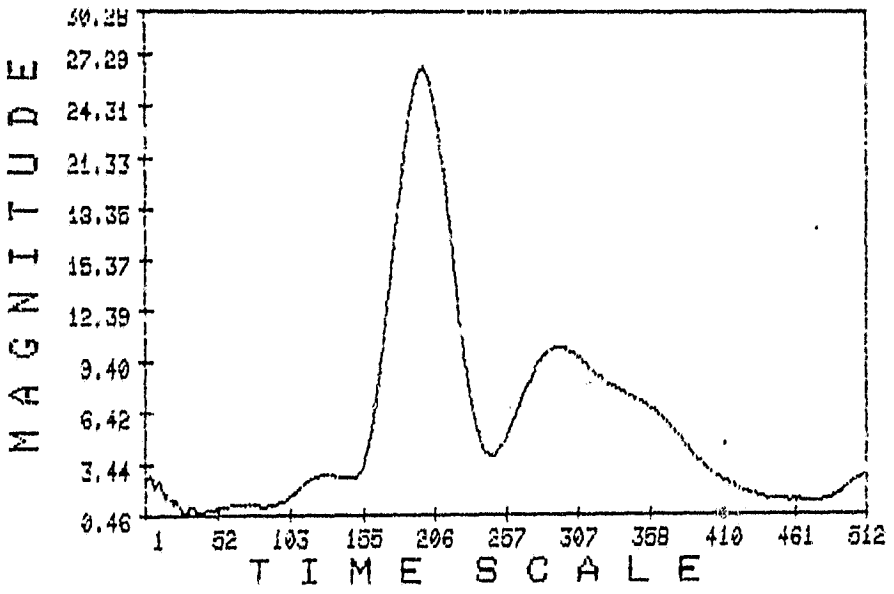


Figure 34. Standard deviation of the received signals from file P0401B (see parameter descriptions in Table 4).

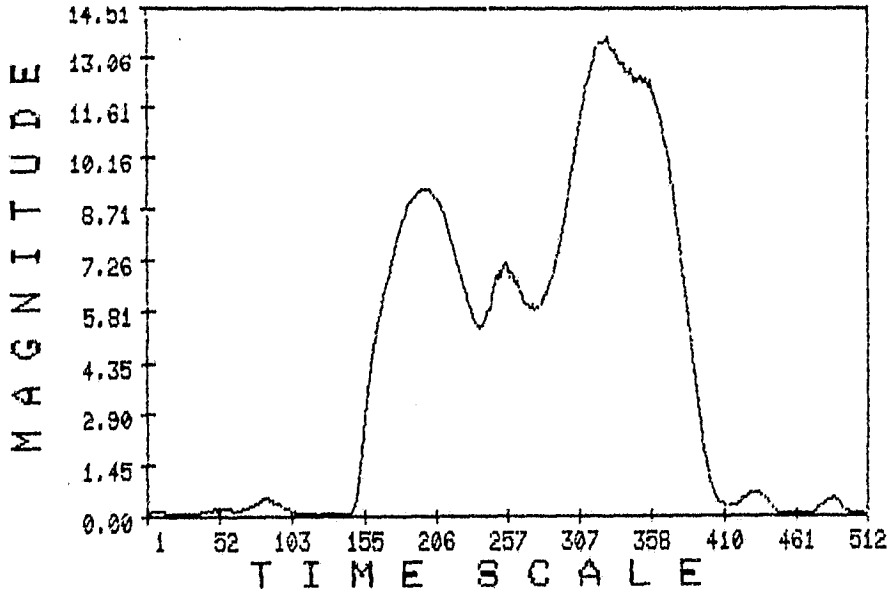


Figure 35. Signal-to-noise ratio of the received signals from file P0401B (see parameter descriptions in Table 4).

ORIGINAL PAGE IS
OF POOR QUALITY



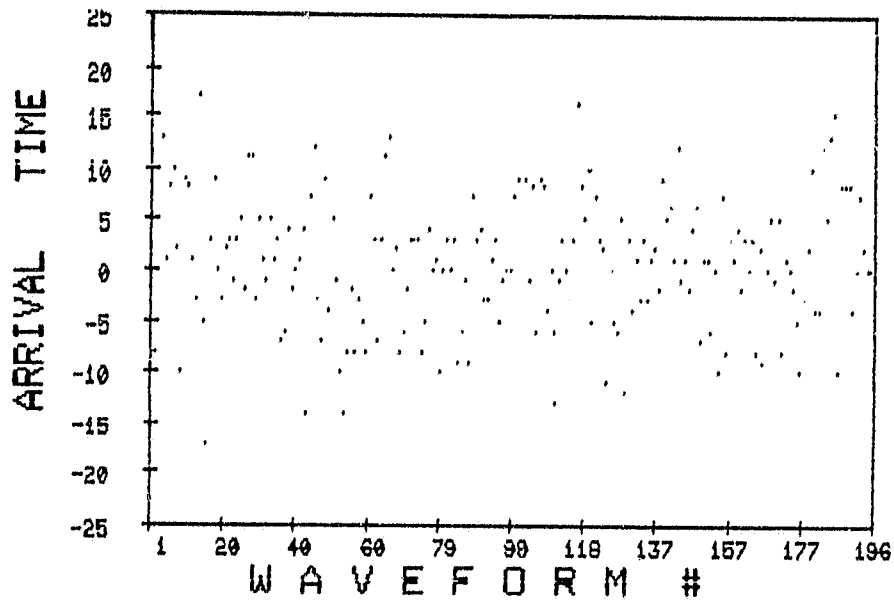


Figure 36. History of the arrival times of the received signals from file P0401B (see parameter descriptions in Table 4).

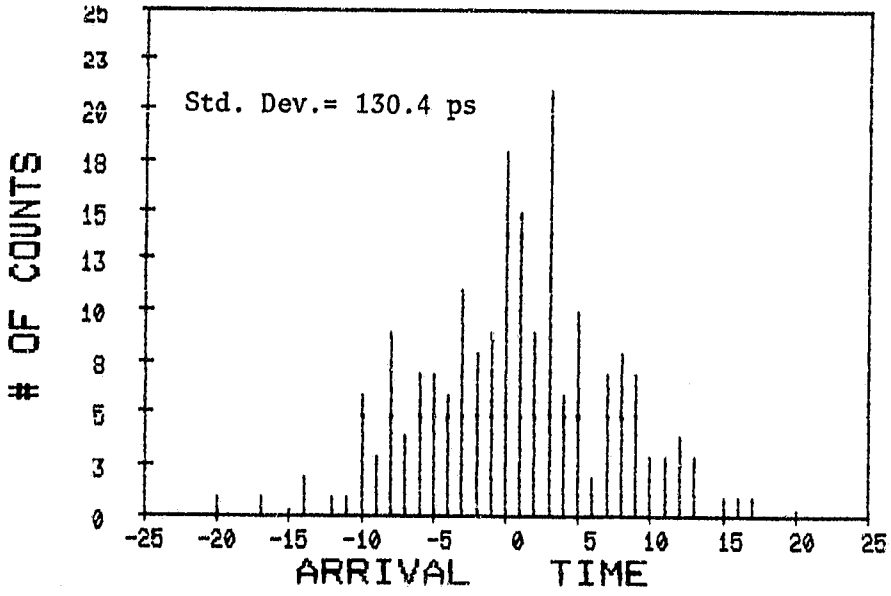


Figure 37. Histogram of the arrival times of the received signals from file P0401B : number of waveforms vs. arrival time (see parameter descriptions in Table 4).

ORIGINAL PAGE IS
OF POOR QUALITY

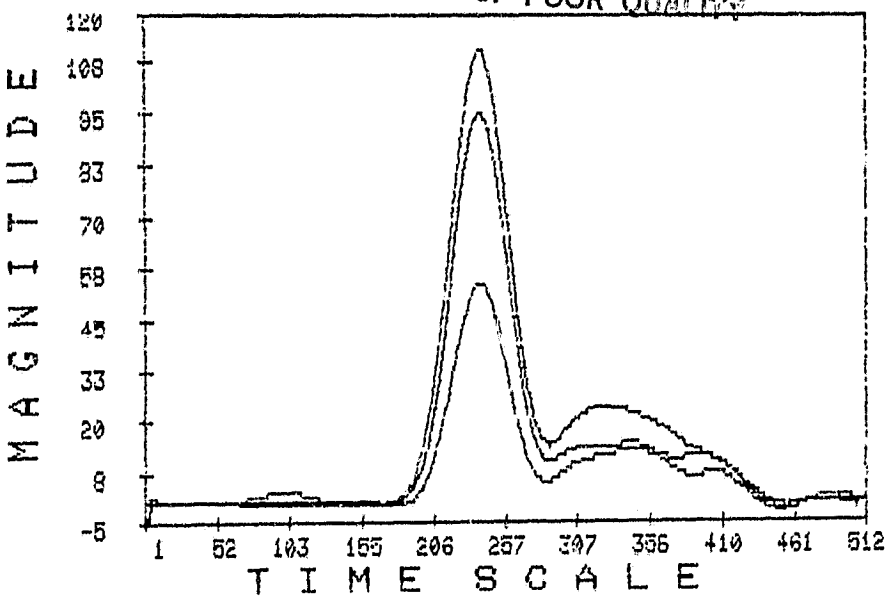


Figure 38. Sample waveforms of the received signals after alignment from file P0401C (see parameter descriptions in Table 4).

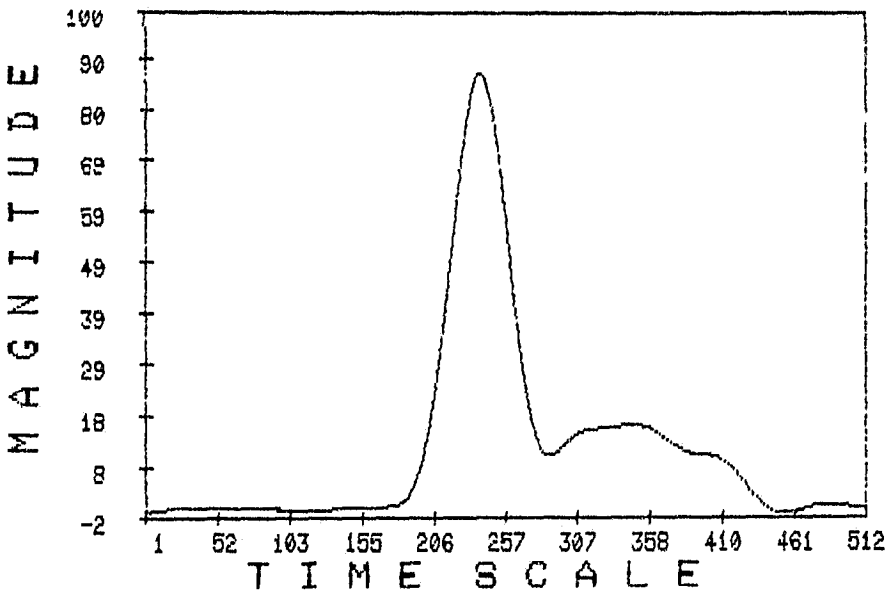


Figure 39. Mean received signal from file P0401C (see parameter descriptions in Table 4).

ORIGINAL PAGE IS
OF POOR QUALITY



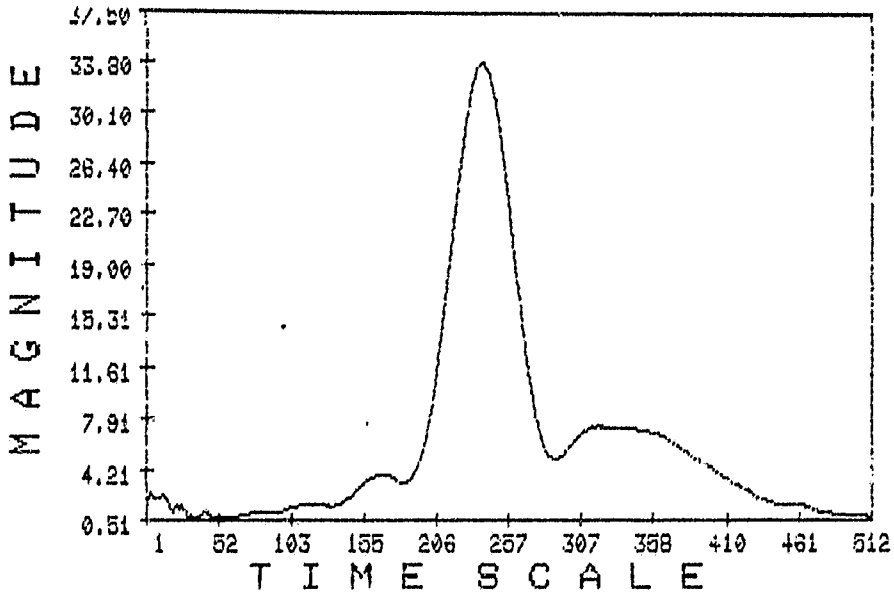


Figure 40. Standard deviation of the received signals from file P0401C (see parameter descriptions in Table 4).

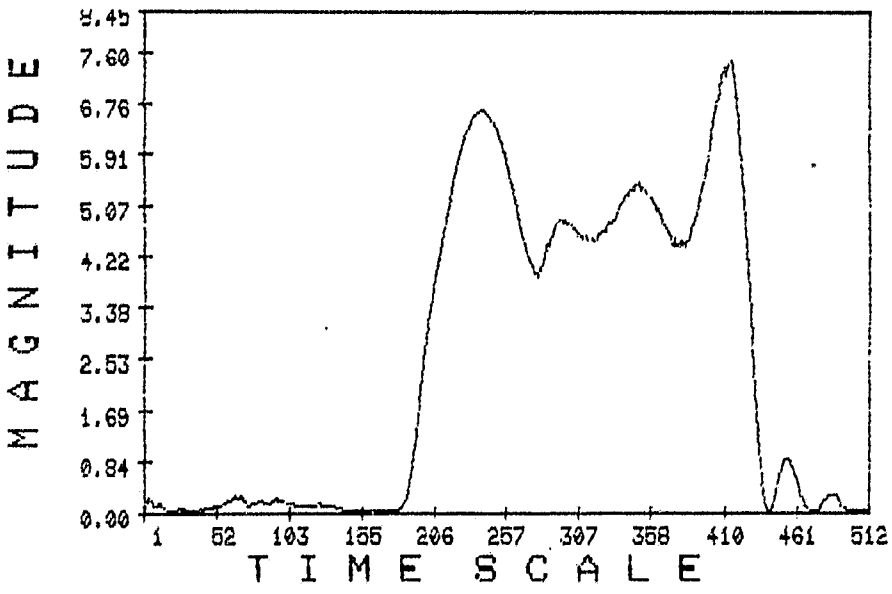


Figure 41. Signal-to-noise ratio of the received signals from file P0401C (see parameter descriptions in Table 4).

ORIGINAL PAGE IS
OF POOR QUALITY



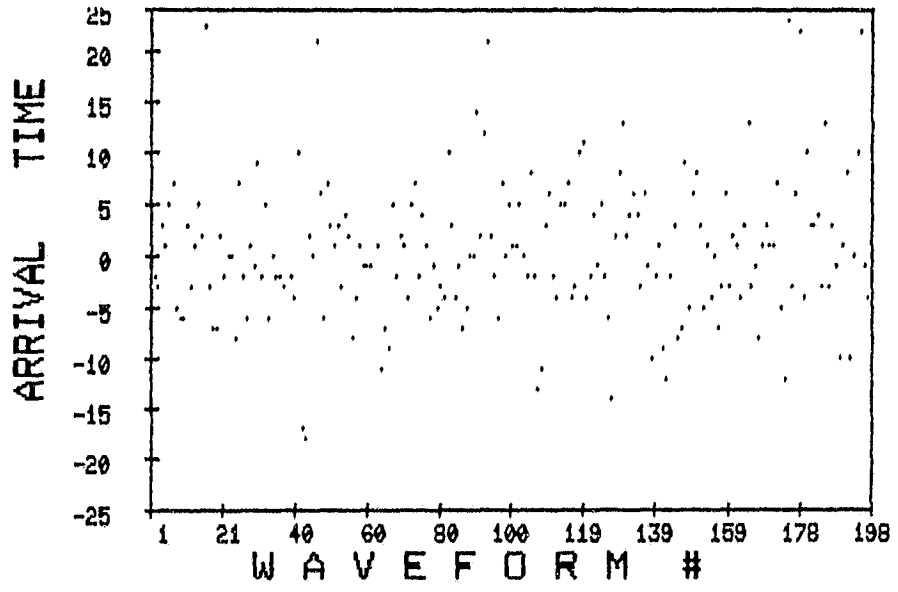


Figure 42. History of the arrival times of the received signals from file P0401C (see parameter descriptions in Table 4).

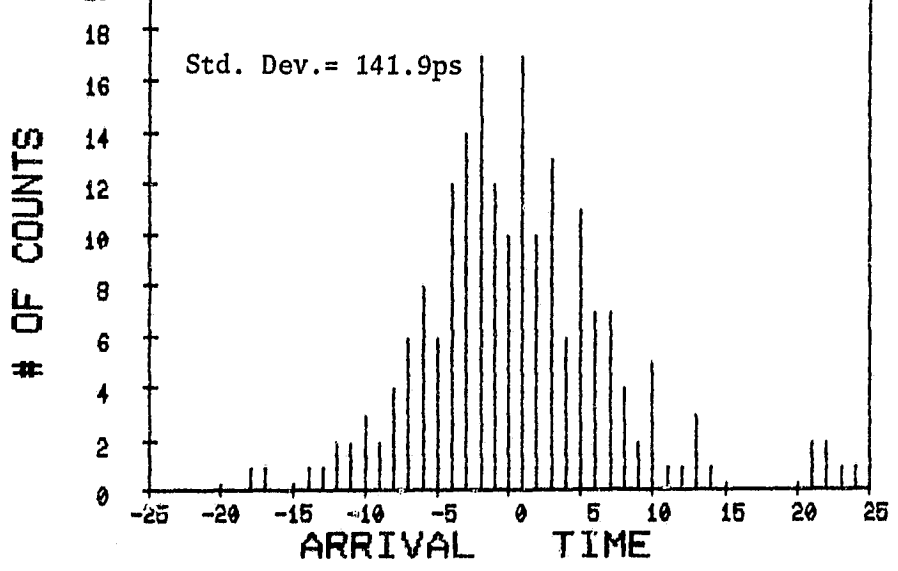


Figure 43. Histogram of the arrival times of the received signals from file P0401C : number of waveforms vs. arrival time (see parameter descriptions in Table 4).

ORIGINAL PAGE IS
OF POOR QUALITY



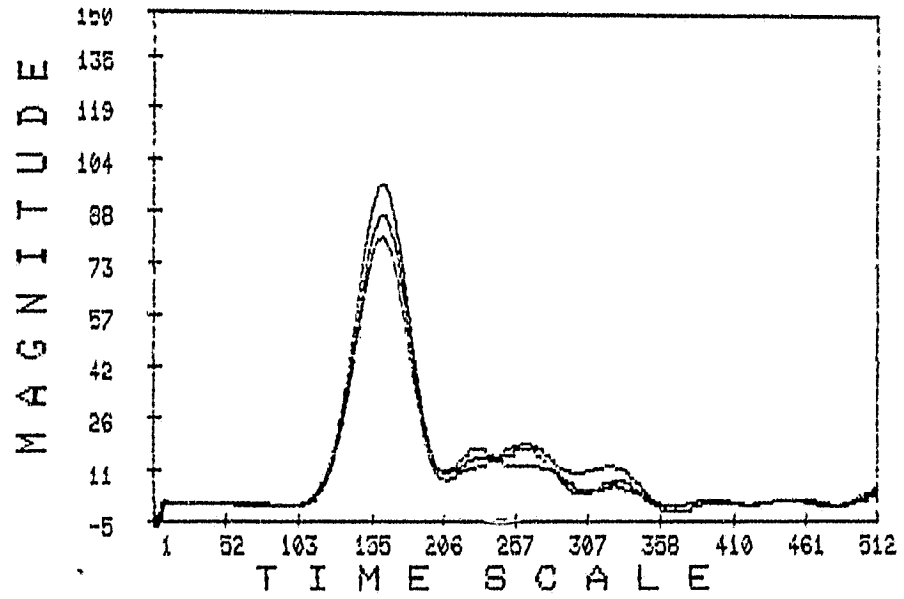


Figure 44. Sample waveforms of the received signals after alignment from file P0401D (see parameter descriptions in Table 4).

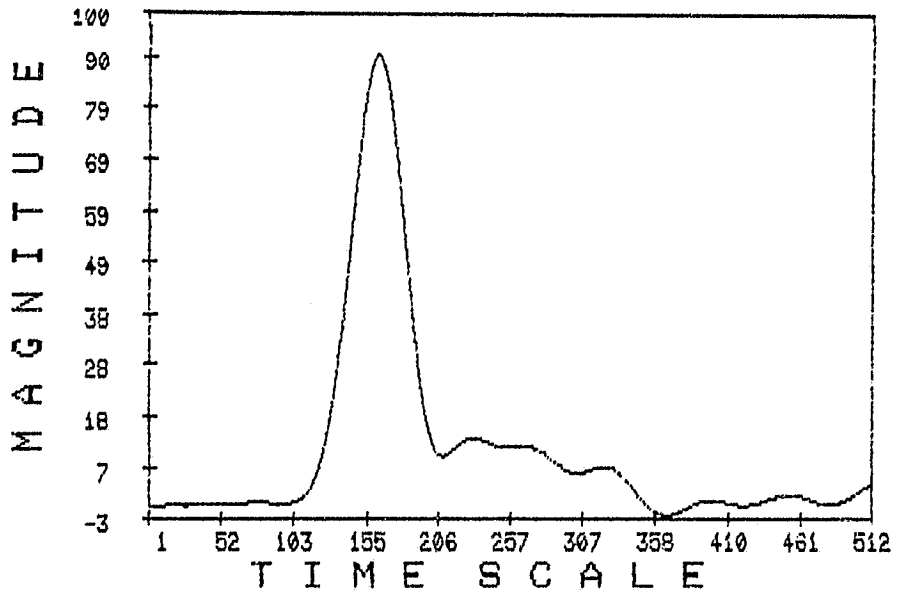


Figure 45. Mean received signal from file P0401D (see parameter descriptions in Table 4).

ORIGINAL PAGE IS
OF POOR QUALITY



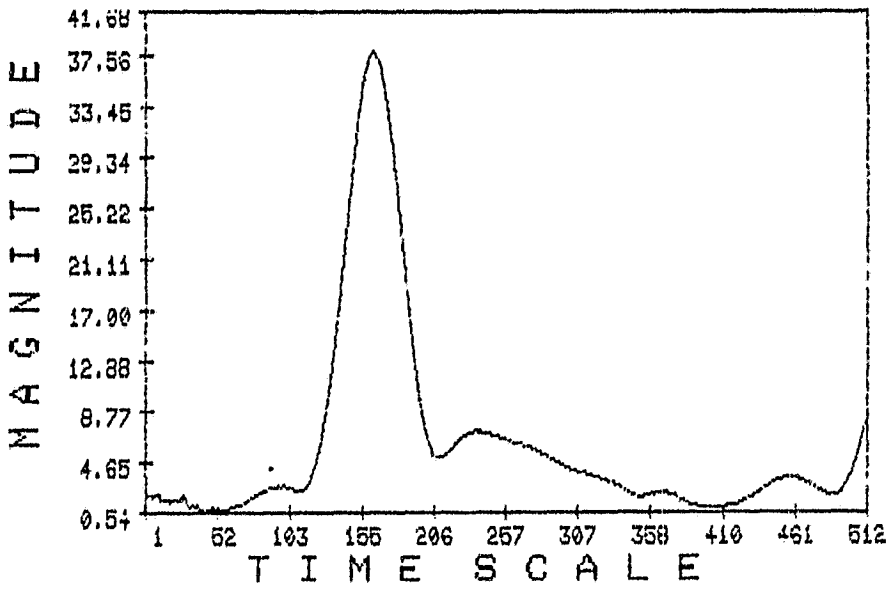


Figure 46. Standard deviation of the received signals from file P0401D (see parameter descriptions in Table 4).

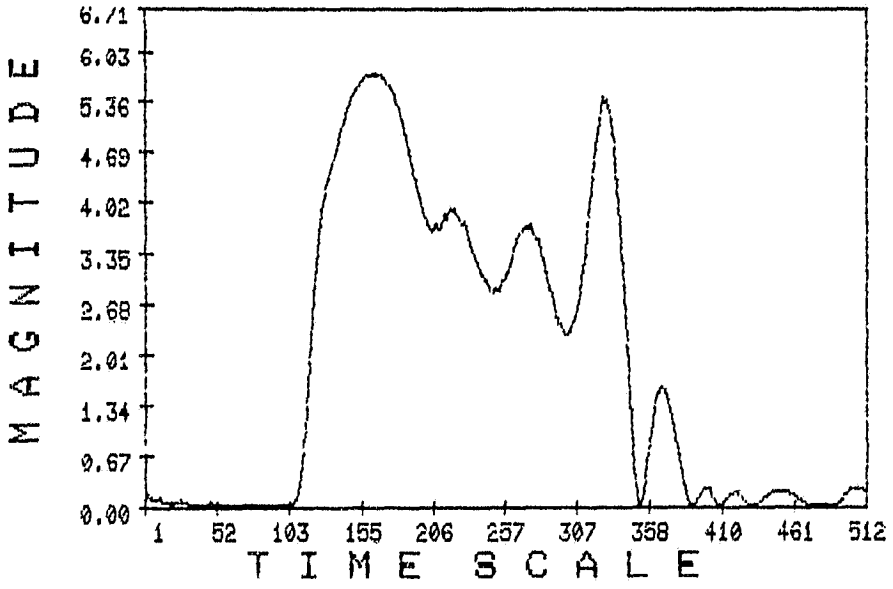


Figure 47. Signal-to-noise ratio of the received signals from file P0401D (see parameter descriptions in Table 4).

ORIGINAL PAGE IS
OF POOR QUALITY



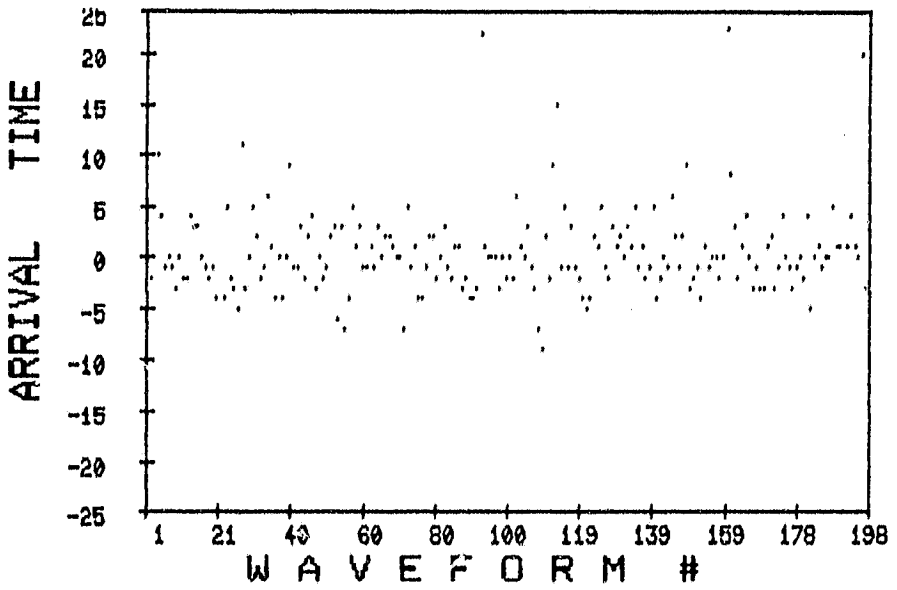


Figure 48. History of the arrival times of the received signals from file P0401D (see parameter descriptions in Table 4).

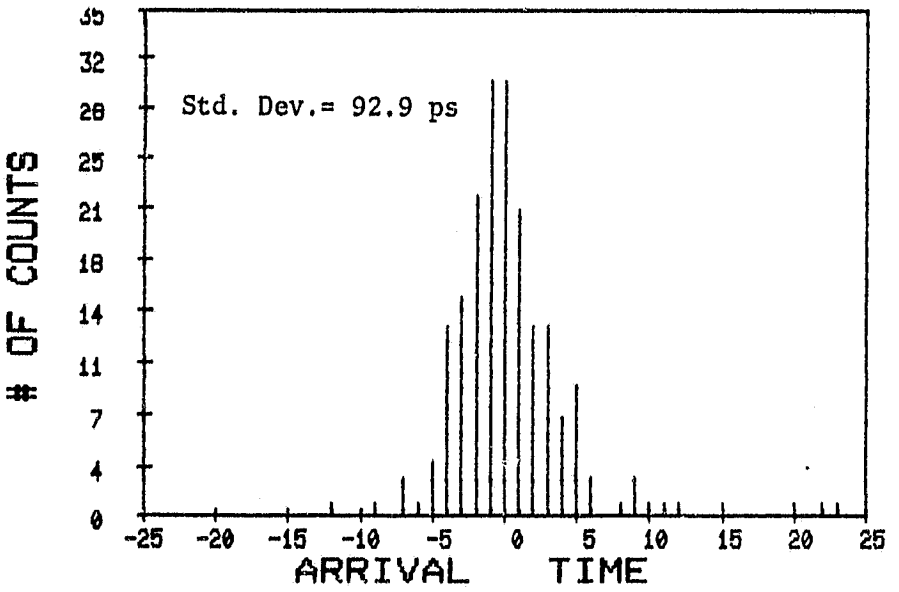


Figure 49. Histogram of the arrival times of the received signals from file P0401D : number of waveforms vs. arrival time (see parameter descriptions in Table 4).

ORIGINAL PAGE IS
OF POOR QUALITY



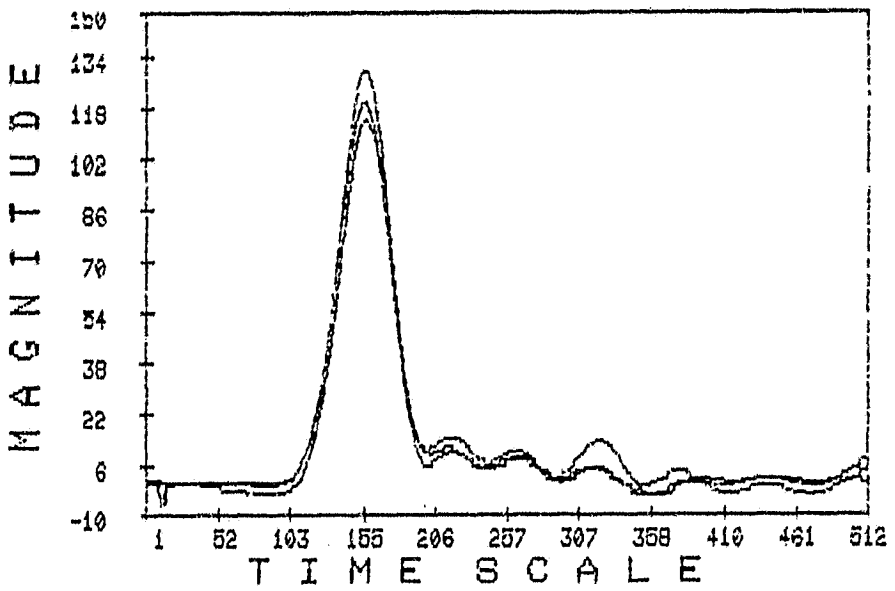


Figure 50. Sample waveforms of the received signals after alignment from file P0401E (see parameter descriptions in Table 4).

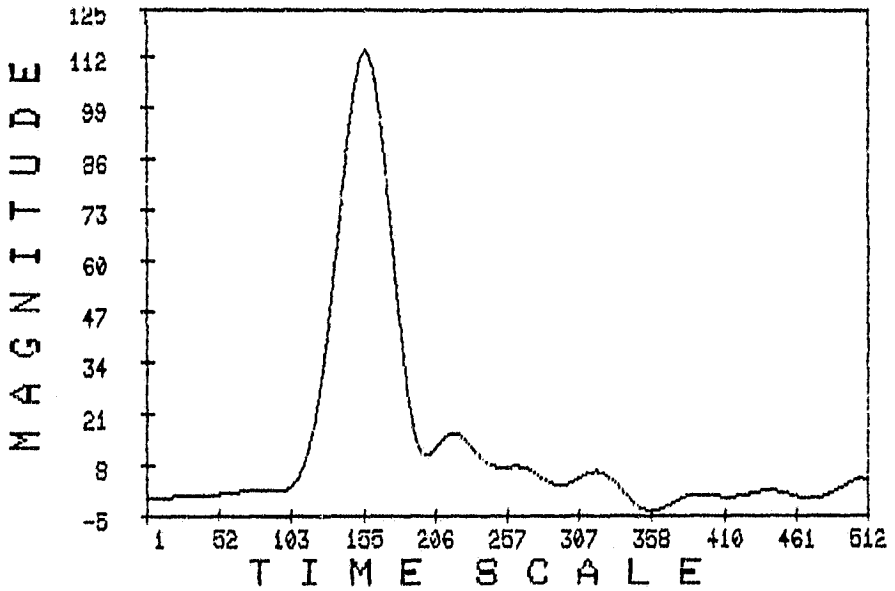


Figure 51. Mean received signal from file P0401E (see parameter descriptions in Table 4).

ORIGINAL PAGE IS
OF POOR QUALITY



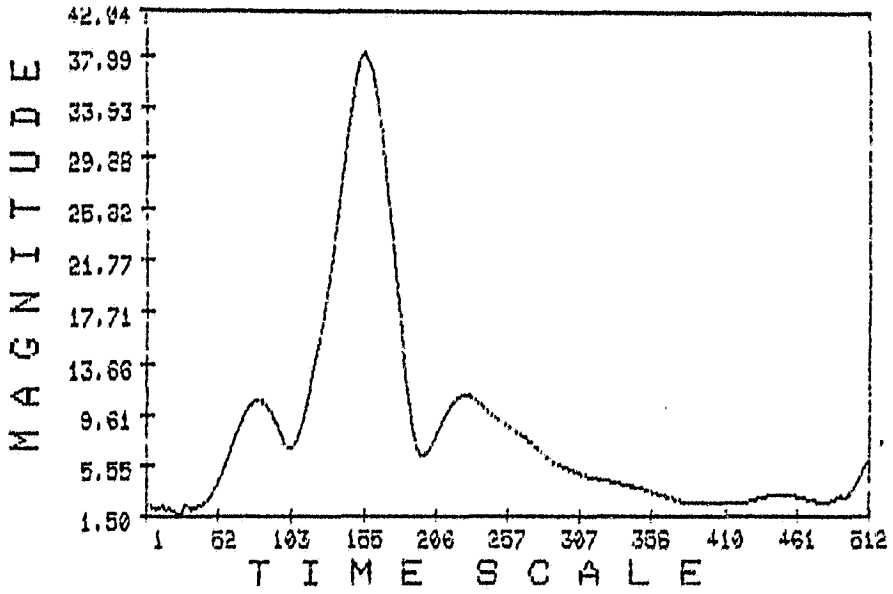


Figure 52. Standard deviation of the received signals from file P0401E (see parameter descriptions in Table 4).

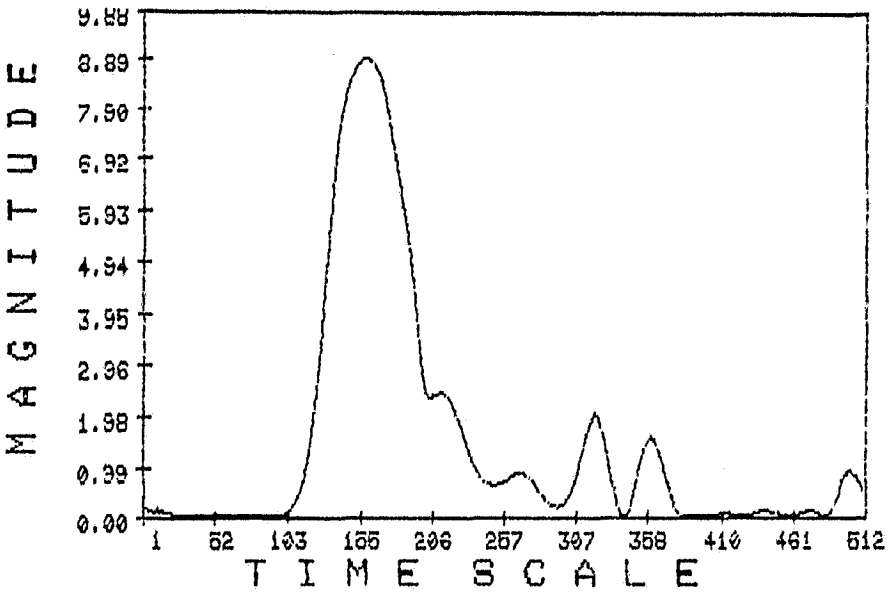


Figure 53. Signal-to-noise ratio of the received signals from file P0401E (see parameter descriptions in Table 4).

ORIGINAL PAGE IS
OF POOR QUALITY



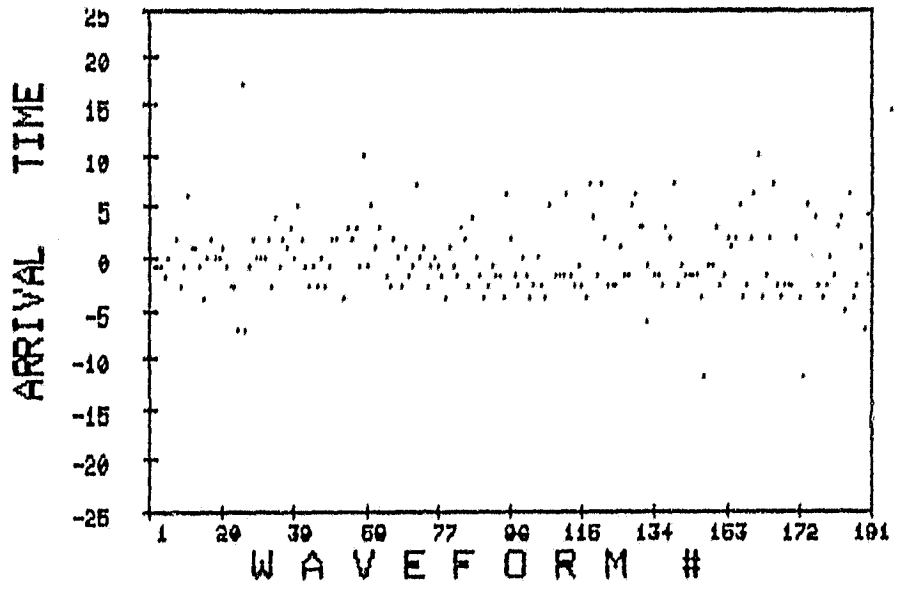


Figure 54. History of the arrival times of the received signals from file P0401E (see parameter descriptions in Table 4).

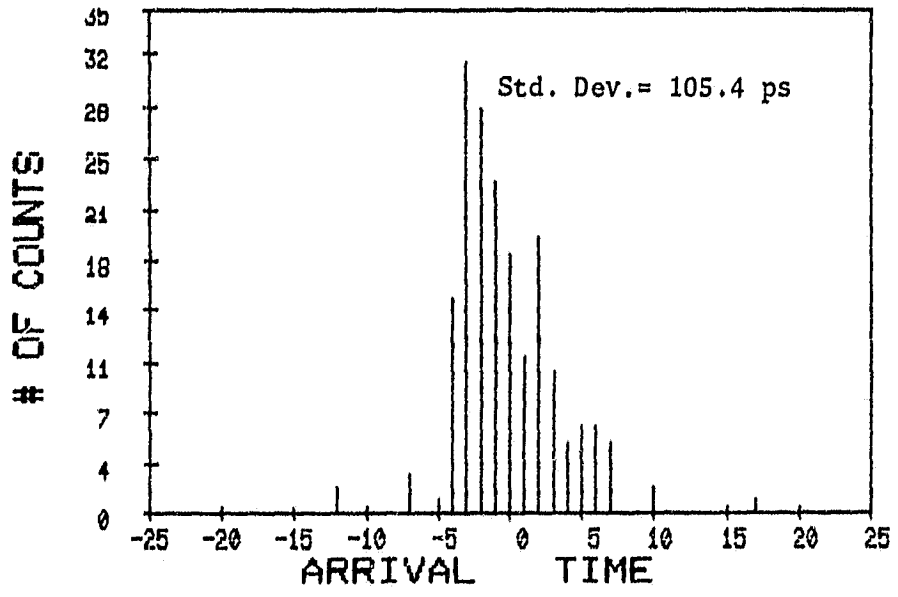


Figure 55. Histogram of the arrival times of the received signals from file P0401E : number of waveforms vs. arrival time (see parameter descriptions in Table 4).

ORIGINAL PAGE IS
OF POOR QUALITY



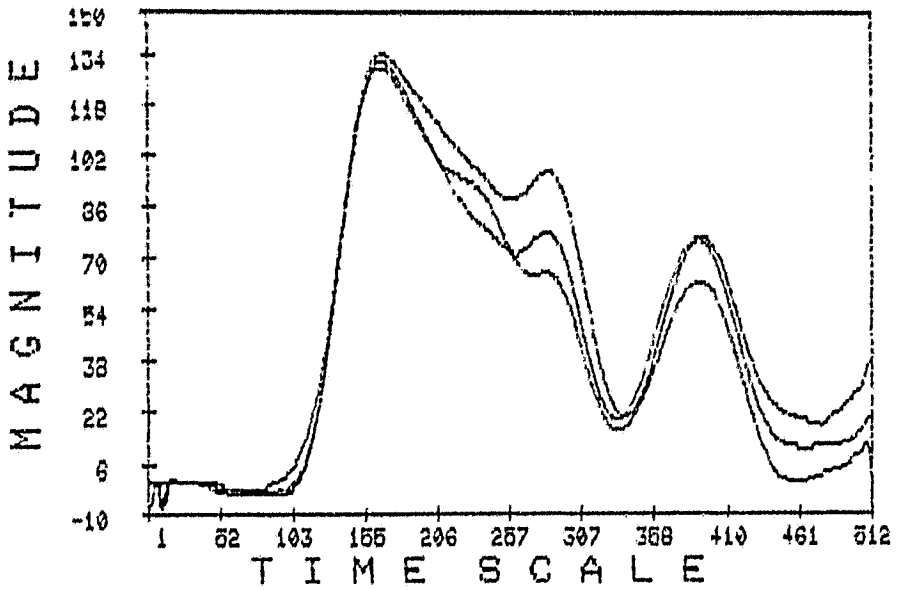


Figure 56. Sample waveforms of the received signals after alignment from file T0331A (see parameter descriptions in Table 4).

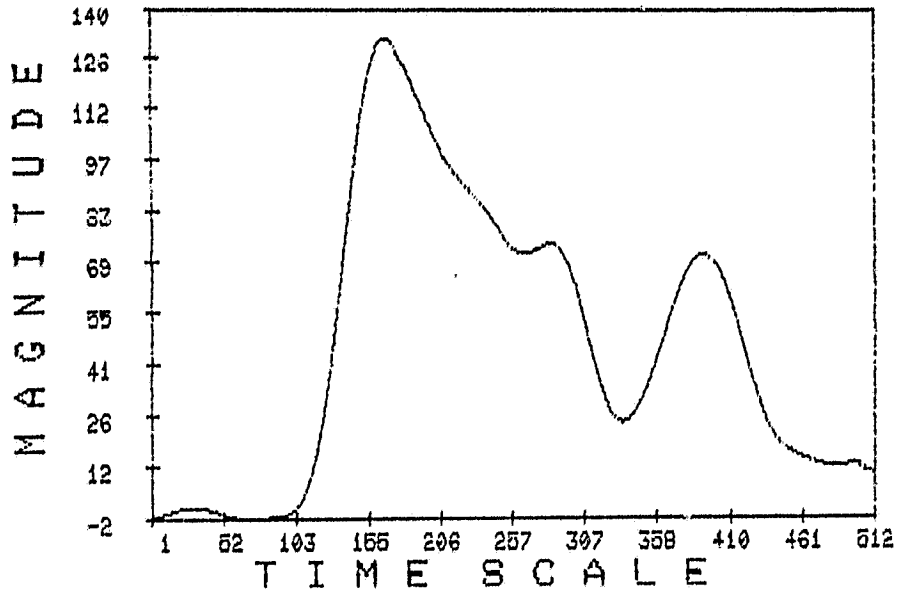


Figure 57. Mean received signal from file T0331A (see parameter descriptions in Table 4).

ORIGINAL PAGE IS
OF POOR QUALITY



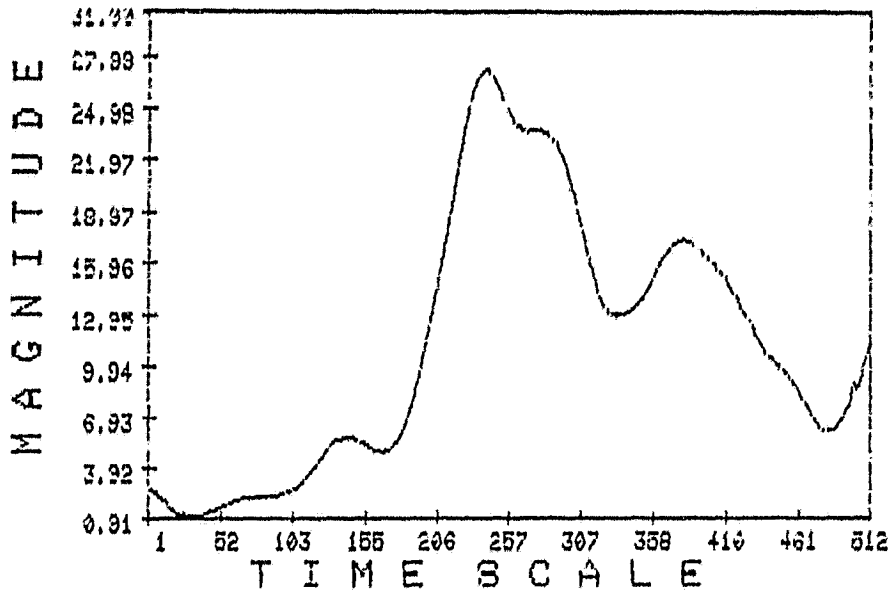


Figure 58. Standard deviation of the received signals from file T0331A (see parameter descriptions in Table 4).

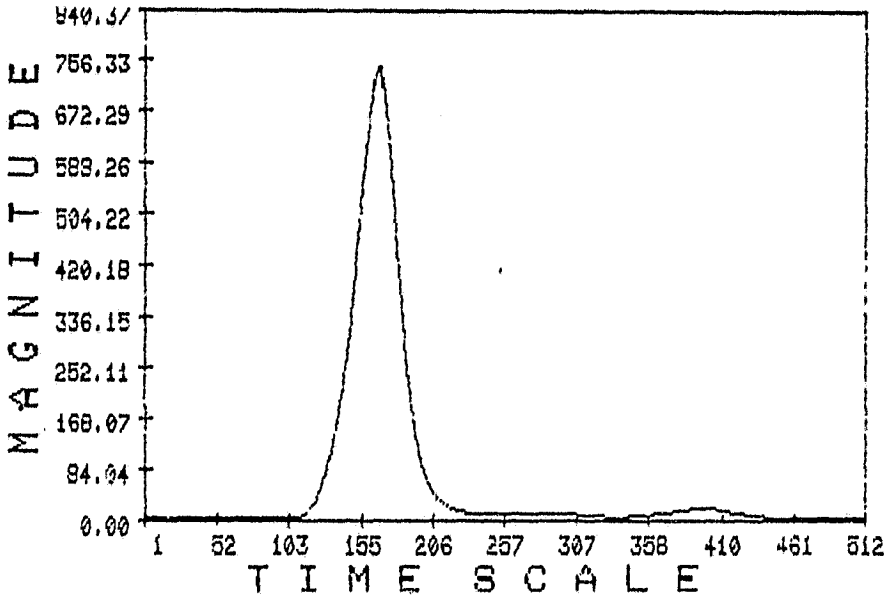


Figure 59. Signal-to-noise ratio of the received signals from file T0331A (see parameter descriptions in Table 4).

ORIGINAL PAGE IS
OF POOR QUALITY



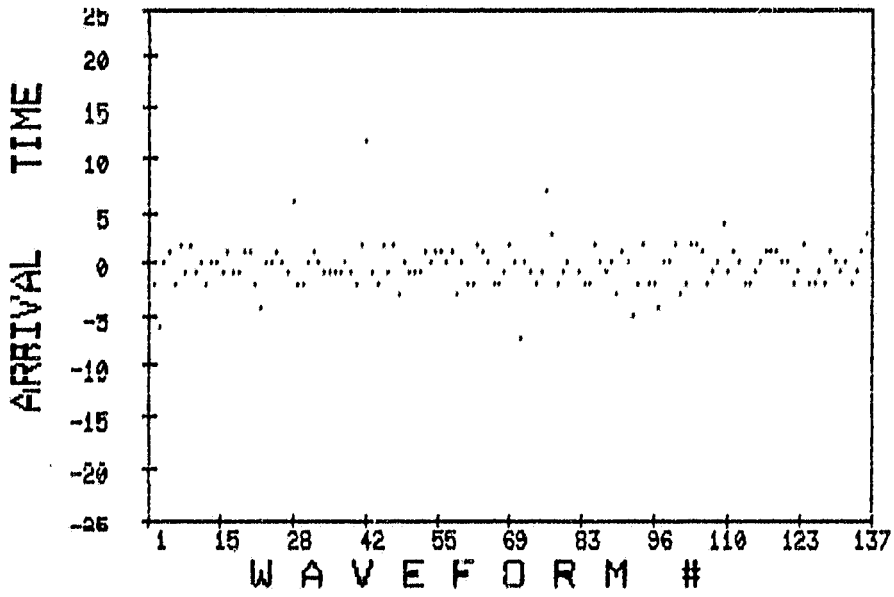


Figure 60. History of the arrival times of the received signals from file T0331A (see parameter descriptions in Table 4).

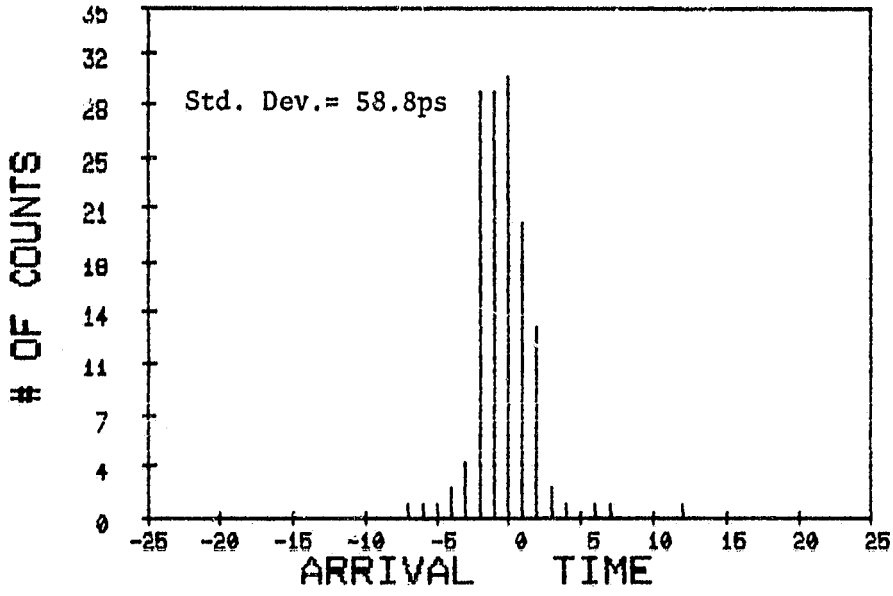


Figure 61. Histogram of the arrival times of the received signals from file T0331A : number of waveforms vs. arrival time (see parameter descriptions in Table 4).

ORIGINAL PAGE IS
OF POOR QUALITY



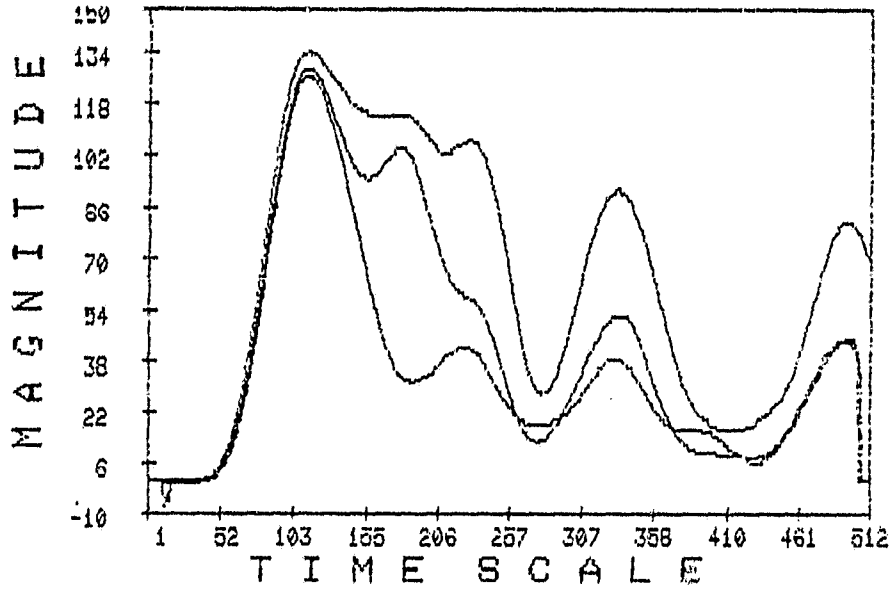


Figure 62. Sample waveforms of the received signals after alignment from file T0331B (see parameter descriptions in Table 4).

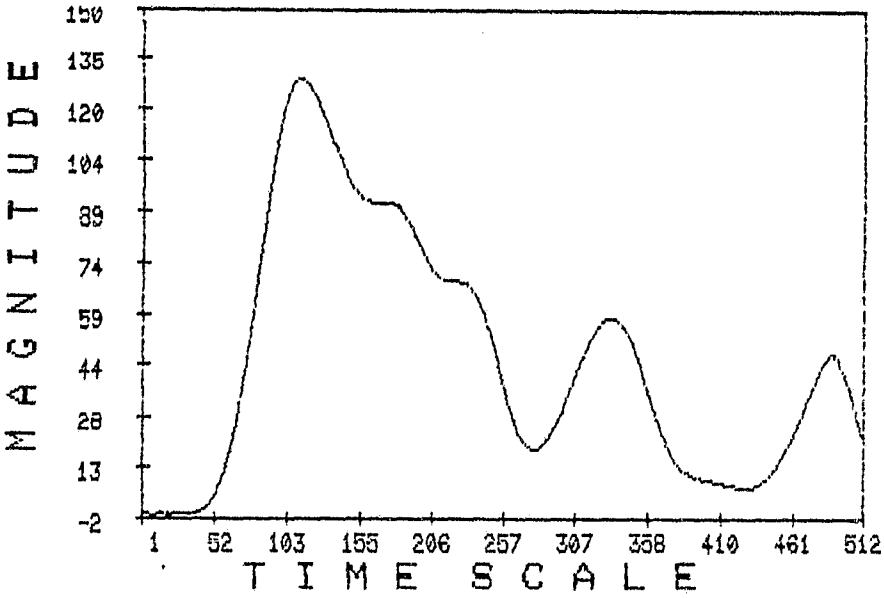


Figure 63. Mean received signal from file T0331B (see parameter descriptions in Table 4).

ORIGINAL PAGE IS
OF POOR QUALITY



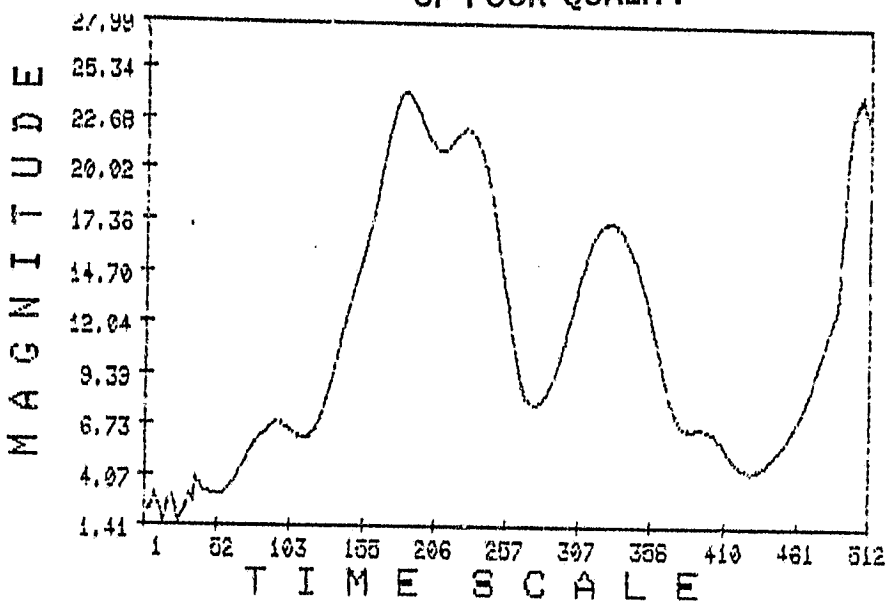


Figure 64. Standard deviation of the received signals from file T0331B (see parameter descriptions in Table 4).

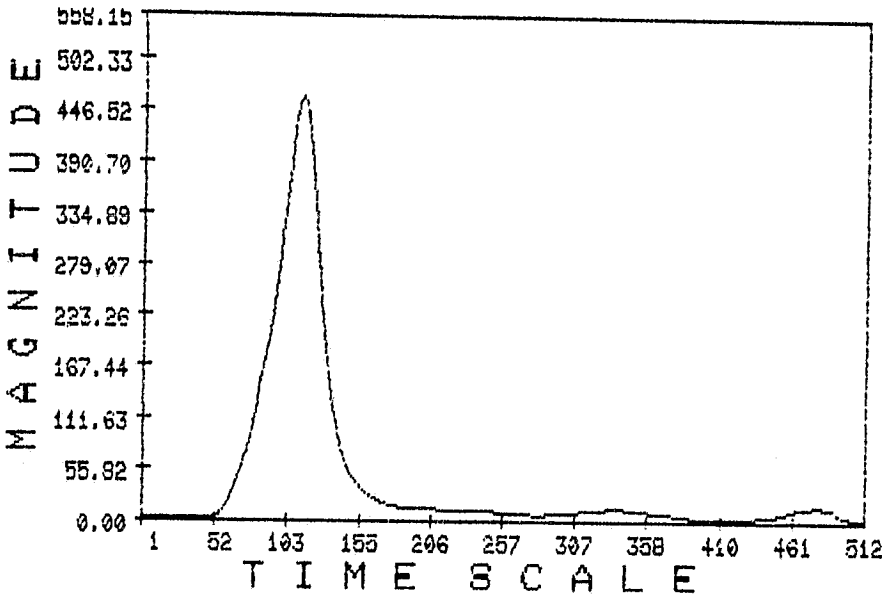


Figure 65. Signal-to-noise ratio of the received signals from file T0331B (see parameter descriptions in Table 4).

ORIGINAL PAGE IS
OF POOR QUALITY



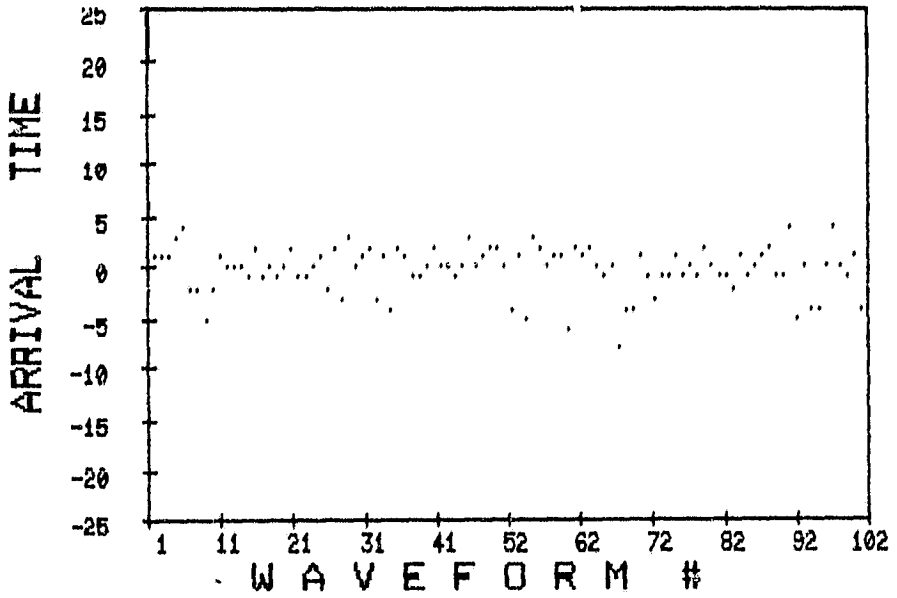


Figure 66. History of the arrival times of the received signals from file T0331B (see parameter descriptions in Table 4).

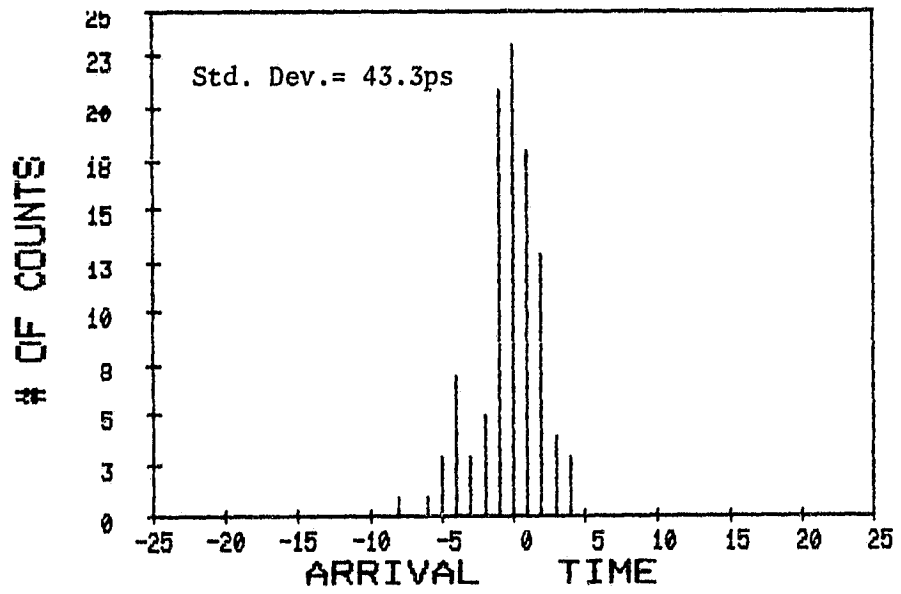


Figure 67. Histogram of the arrival times of the received signals from file T0331B : number of waveforms vs. arrival time (see parameter descriptions in Table 4).

ORIGINAL PAGE IS
OF POOR QUALITY



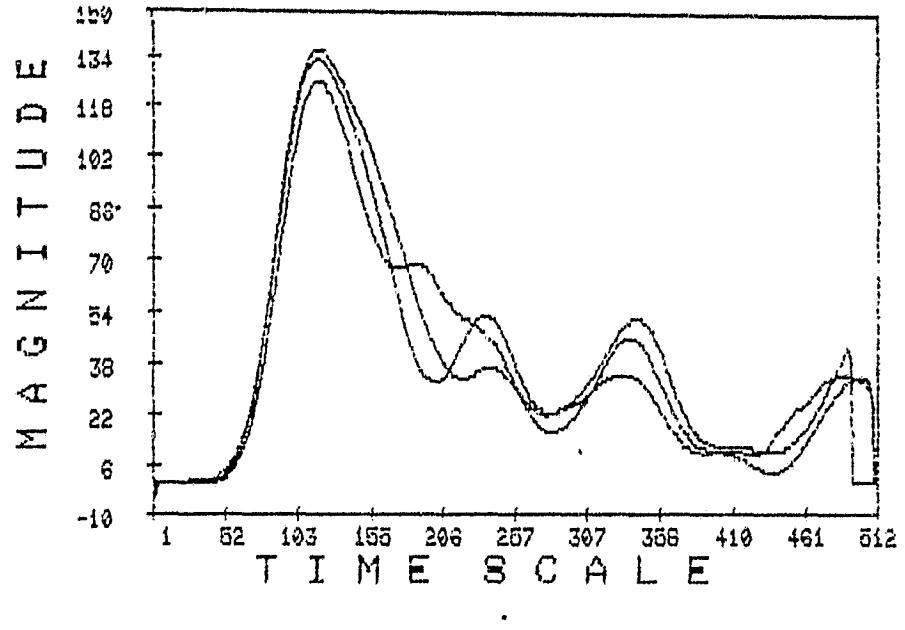


Figure 68. Sample waveforms of the received signals after alignment from file T0331C (see parameter descriptions in Table 4).

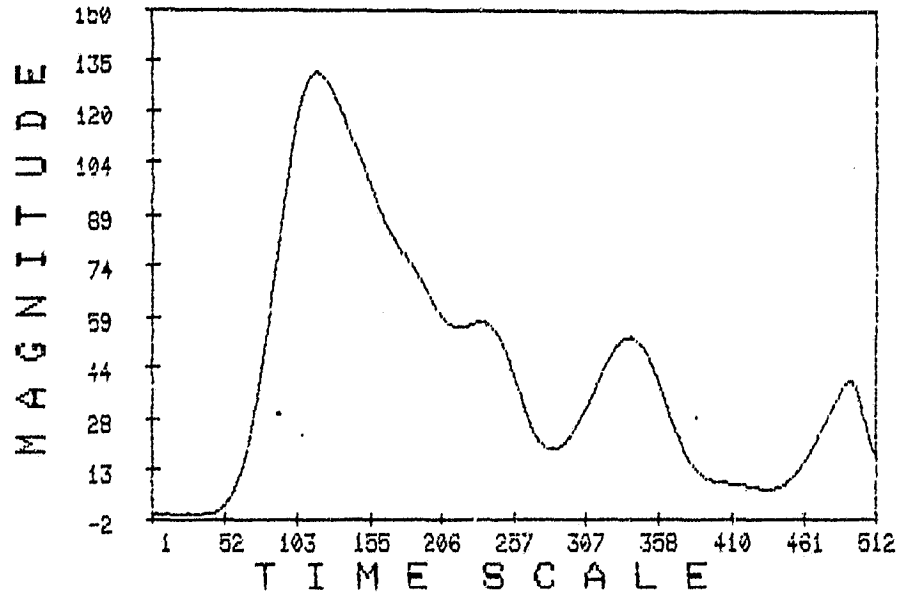


Figure 69. Mean received signal from file T0331C (see parameter descriptions in Table 4).

ORIGINAL PAGE IS
OF POOR QUALITY



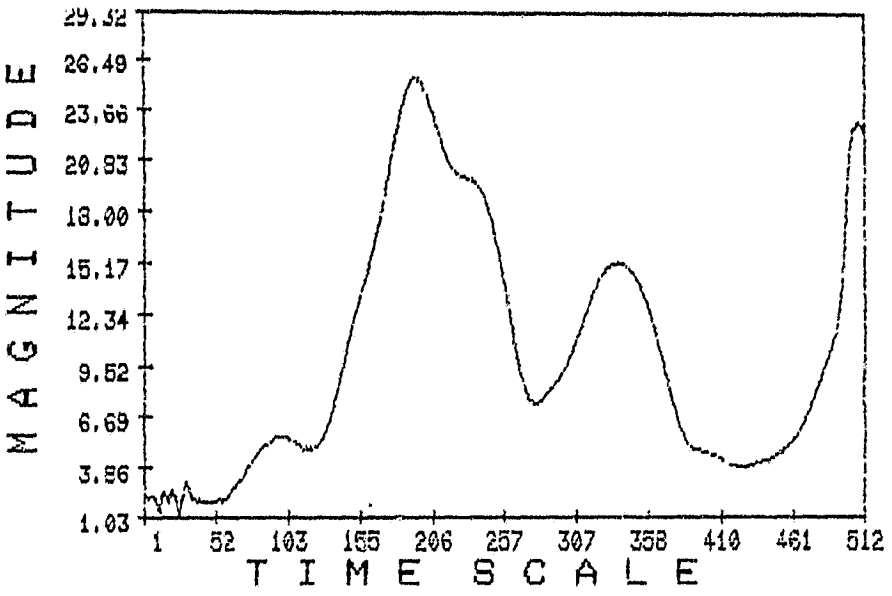


Figure 70. Standard deviation of the received signals from file T0331C (see parameter descriptions in Table 4).

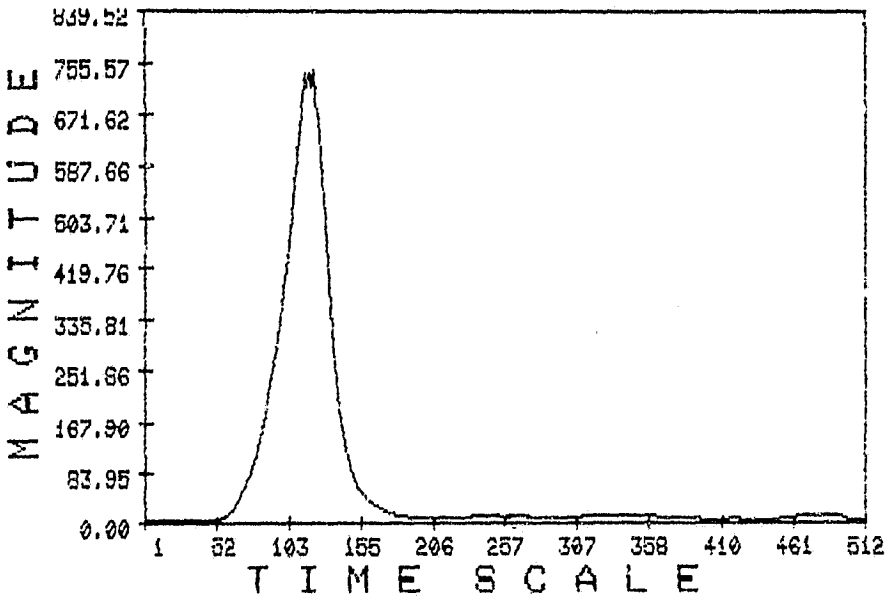


Figure 71. Signal-to-noise ratio of the received signals from file T0331C (see parameter descriptions in Table 4).

ORIGINAL PAGE IS
OF POOR QUALITY



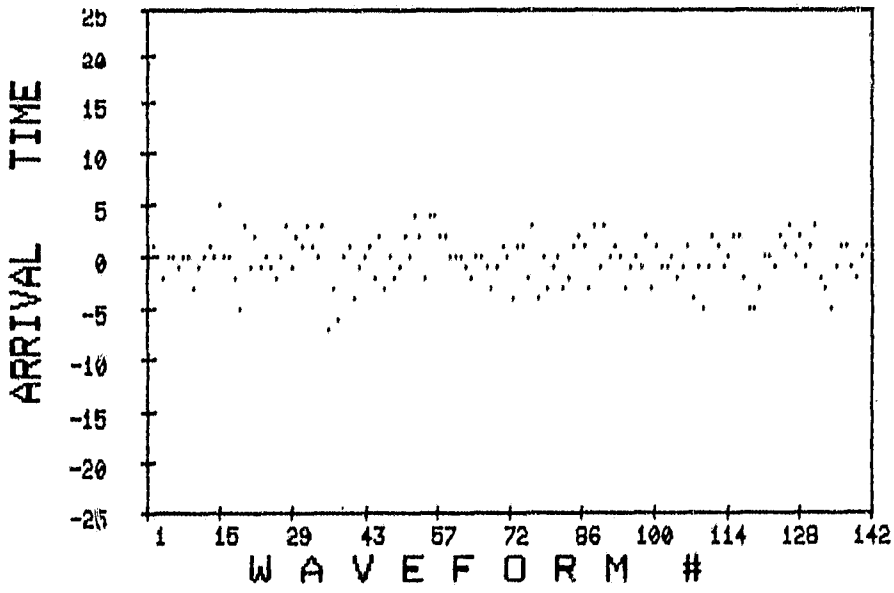


Figure 72. History of the arrival times of the received signals from file T0331C (see parameter descriptions in Table 4).

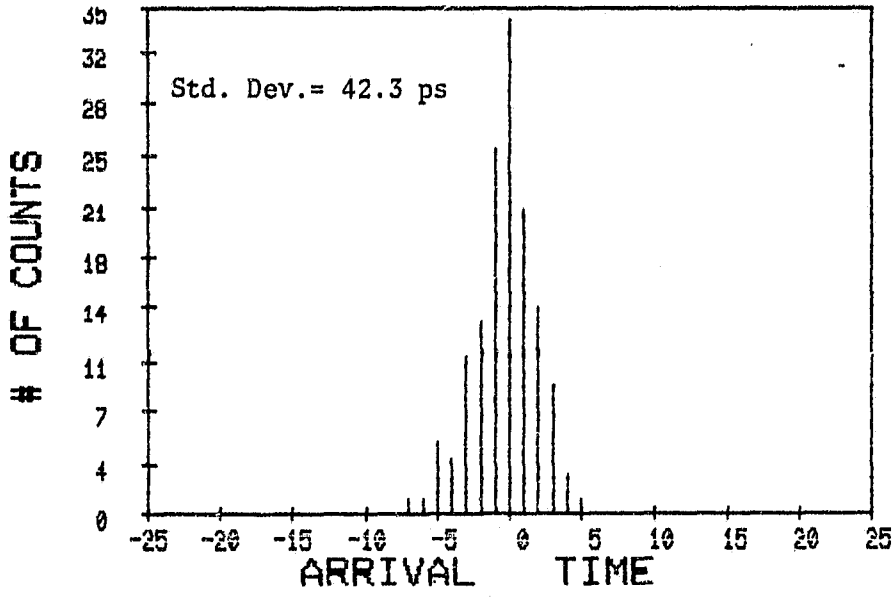


Figure 73. Histogram of the arrival times of the received signals from file T0331C : number of waveforms vs. arrival time (see parameter descriptions in Table 4).

ORIGINAL PAGE IS
OF POOR QUALITY



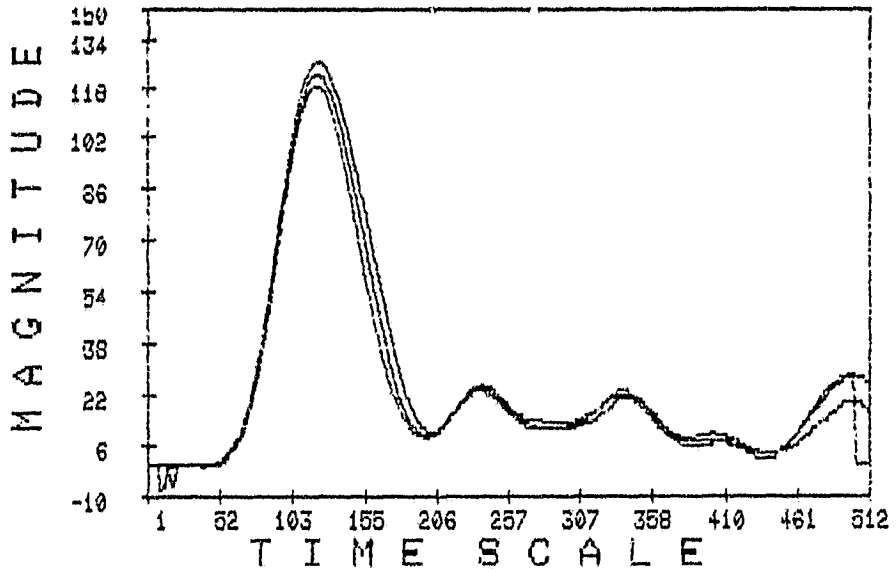


Figure 74. Sample waveforms of the received signals after alignment from file T0331D (see parameter descriptions in Table 4).

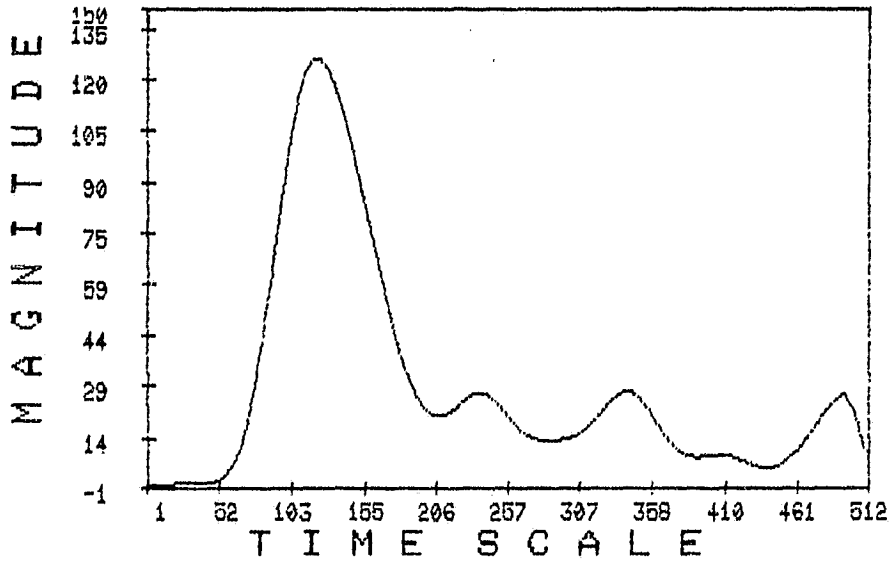


Figure 75. Mean received signal from file T0331D (see parameter descriptions in Table 4).

ORIGINAL PAGE IS
OF POOR QUALITY



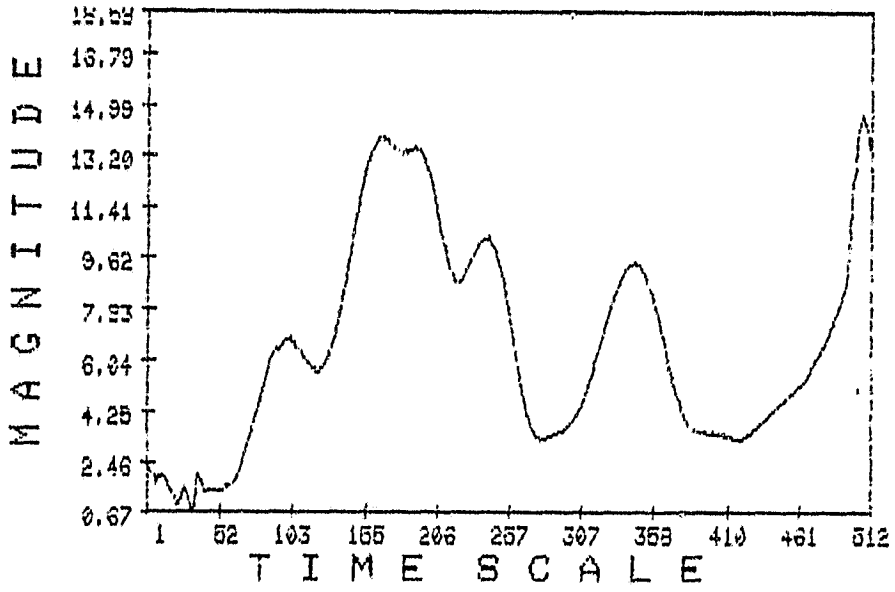


Figure 76. Standard deviation of the received signals from file T0331D (see parameter descriptions in Table 4).

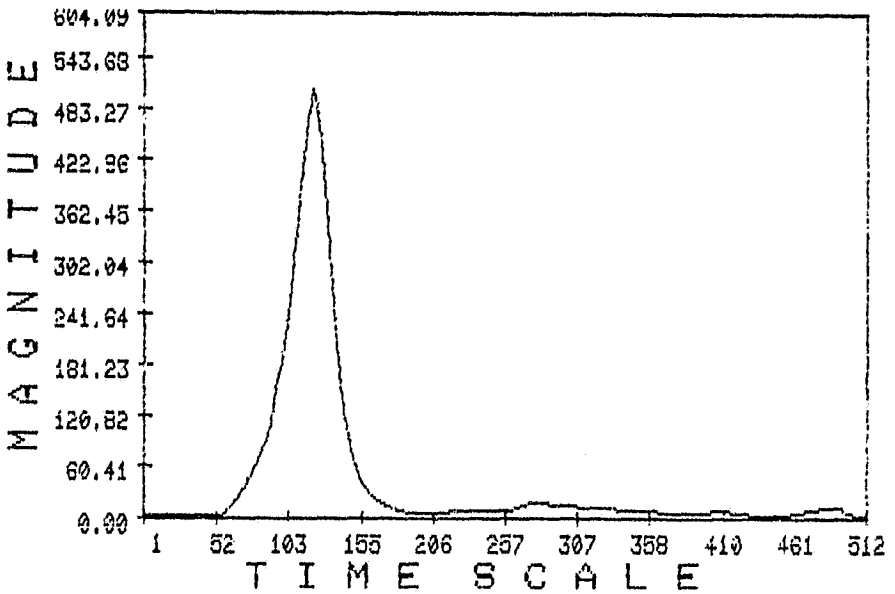


Figure 77. Signal-to-noise ratio of the received signals from file T0331D (see parameter descriptions in Table 4).

ORIGINAL PAGE IS
OF POOR QUALITY



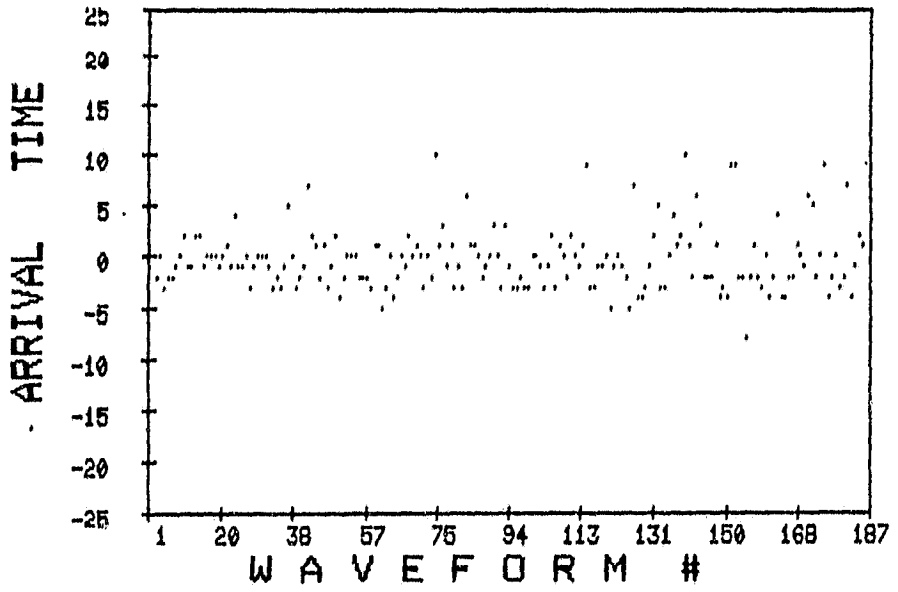


Figure 78. History of the arrival times of the received signals from file T0331D (see parameter descriptions in Table 4).

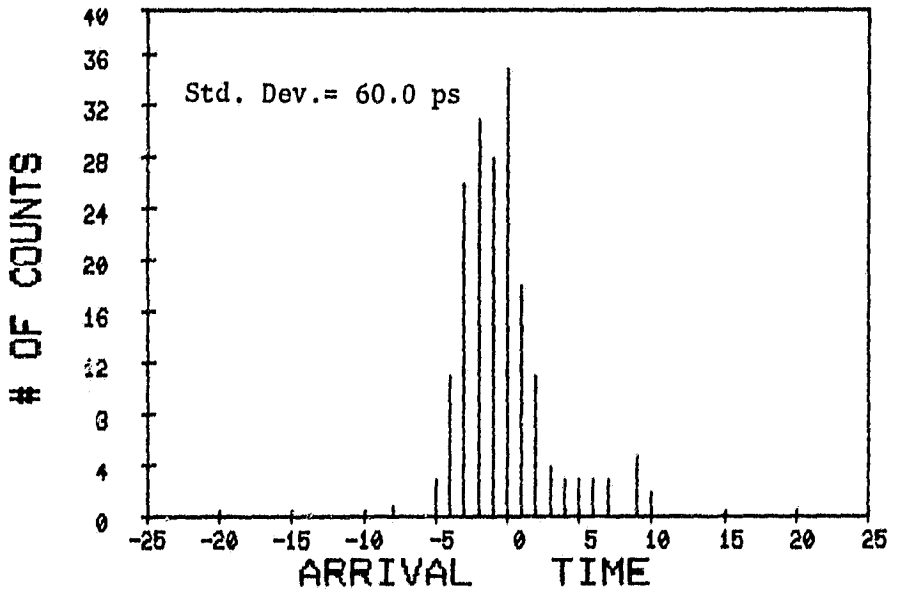


Figure 79. Histogram of the arrival times of the received signals from file T0331D : number of waveforms vs. arrival time (see parameter descriptions in Table 4).

ORIGINAL PAGE IS
OF POOR QUALITY



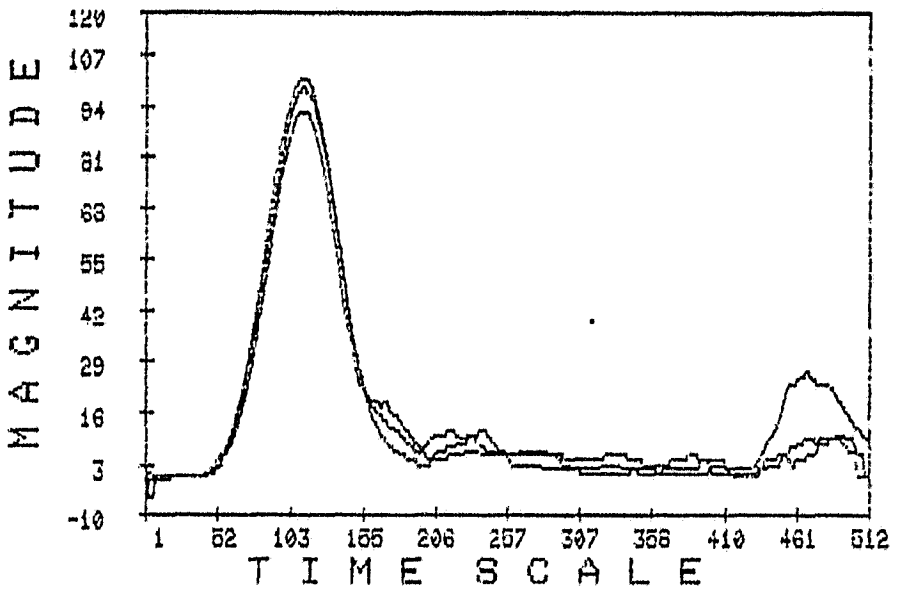


Figure 80. Sample waveforms of the received signals after alignment from file T0331E (see parameter descriptions in Table 4).

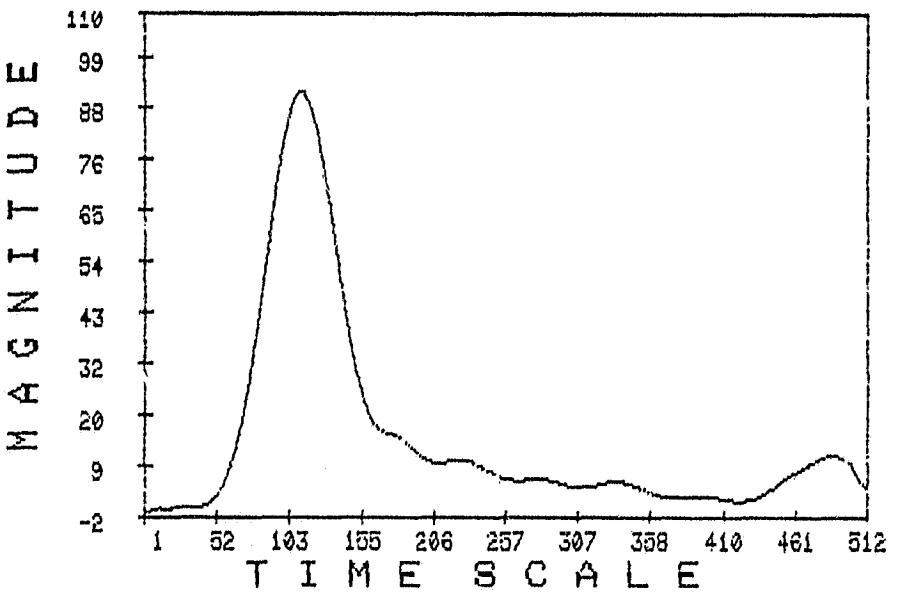


Figure 81. Mean received signal from file T0331E (see parameter descriptions in Table 4).

ORIGINAL PAGE IS
OF POOR QUALITY



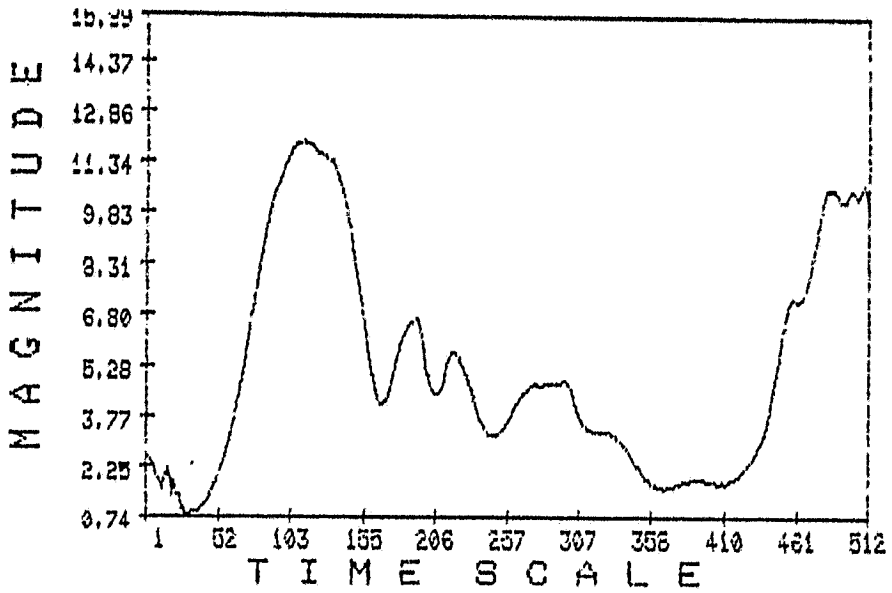


Figure 82. Standard deviation of the received signals from file T0331E (see parameter descriptions in Table 4).

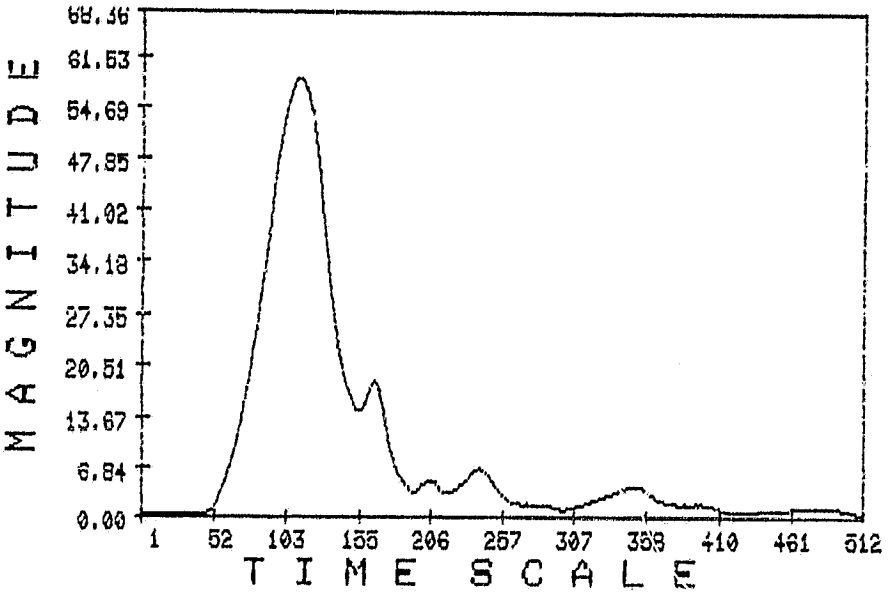


Figure 83. Signal-to-noise ratio of the received signals from file T0331E (see parameter descriptions in Table 4).

ORIGINAL PAGE IS
OF POOR QUALITY



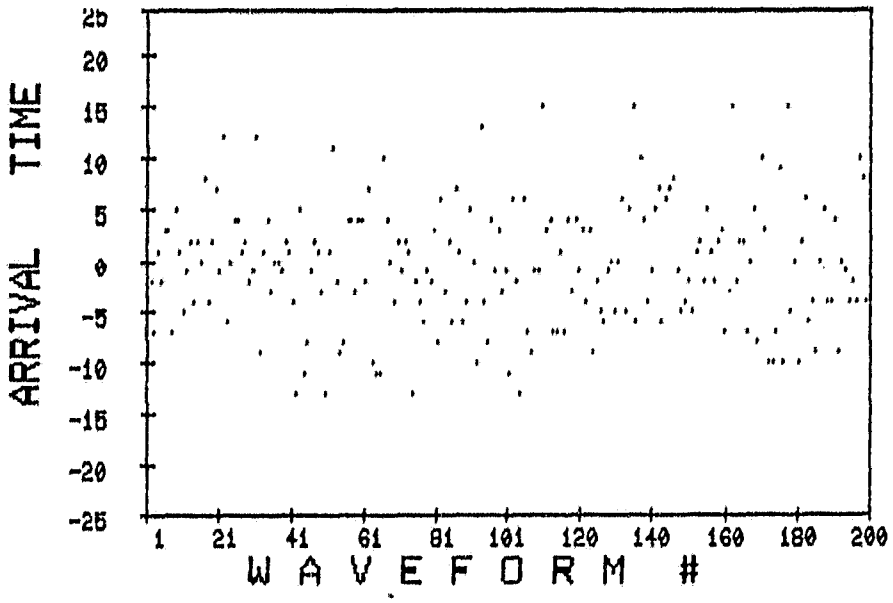


Figure 84. History of the arrival times of the received signals from file T0331E (see parameter descriptions in Table 4).

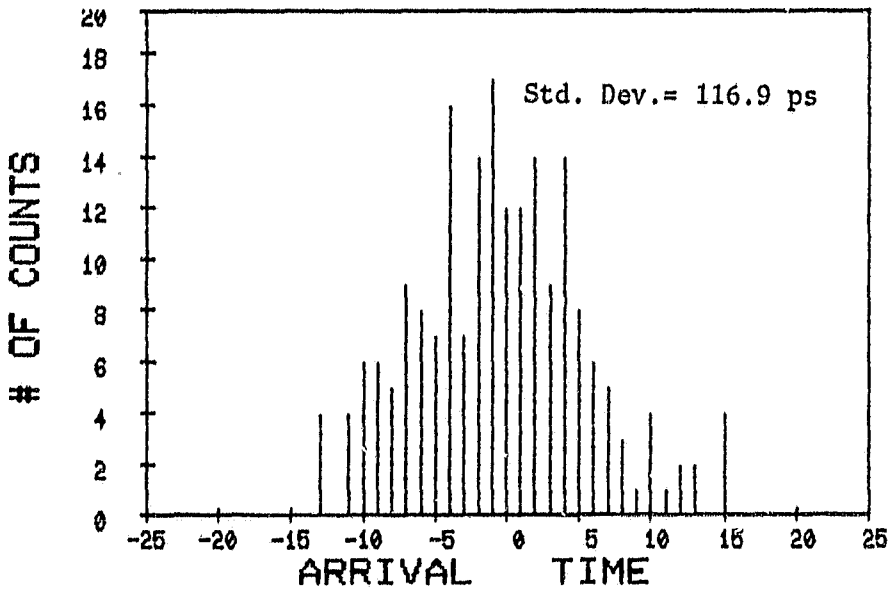


Figure 85. Histogram of the arrival times of the received signals from file T0331E : signal count vs. arrival time (see parameter descriptions in Table 4).

# 5. DATA ANALYSIS

From the experimental results, we observe considerable fluctuations both in time and amplitude in the received signal waveforms. The main sources which contributed to random amplitude fluctuations are fluctuations in laser output energy, shot noise, speckle noise, turbulence, and random gain of the photomultiplier. The main sources of temporal fluctuations are the time jitter in the photomultiplier and waveform digitizer. As mentioned in Chapter 4, the problem of temporal fluctuation was corrected by properly aligning the waveforms using the retro-reflector returns. In this chapter, we concentrate on the problem of amplitude fluctuation and the timing performance of the correlation algorithm.

Due to the nature of the noise sources, there are different types of amplitude fluctuations presented in the laser ranging measurements. Fluctuations in laser output energy and photomultiplier's random gain contribute to fluctuations in the received energy level from pulse to pulse. The effects of turbulence and shot noise cause fluctuations in energy level and distortion of the received pulse shape. The effect of speckle noise on the extended target-returns causes both fluctuations in energy level and small-scale fluctuations within each received pulse.

The retro-reflector has an optically smooth surface, so its returns are free of speckle noise-induced fluctuations. Also, because it is a point target, the problem of pulse distortion is nonexistent. This fact is well-illustrated by referring to the recorded waveforms. In these waveforms, the retro-reflector returns have very smooth Gaussian shapes with widths

equal to the impulse response of the receiver. The variations in energy levels among them are due to other noise sources.

By comparing the returns from the extended targets with those from the retro-reflector, we find that the returns from the extended targets drop off much faster than those from the retro-reflector as the receiving aperture area decreases. This is because the optically rough surfaces of the extended targets cause the reflected beam to scatter. The portion of the scattered beam being intercepted by the receiving telescope also spreads over the entire aperture, and so any changes in the aperture area will cause the changes in the amount of received energy. On the other hand, the reflected beam from the nondispersive retro-reflector is directed right back to the receiver without much divergence, this means a total interception of the reflected beam and the spatial extent of this beam are much smaller than the area of the receiving aperture. Consequently, the returns from the retro-reflector are much less sensitive to the changes in the receiving aperture.

In the plate target configuration, the widths of the returned pulses are broadened by both range spread and curvature effects. Due to the physical size of the receiving aperture, a large number of speckle correlation cells are intercepted by the receiving telescope, or equivalently, the spatial granularity of the returns is very fine with respect to the receiving aperture diameter.[10] This, in turn, implies that the effects of the speckle noise-induced fluctuations are negligible. Also, because of the larger target area, the return energy from the plate target is much less sensitive to the turbulence-induced horizontal beam wandering than that from the retro-reflector. That is the reason for the higher SNR's in the plate target

returns than those in the retro-reflector returns.

The waveforms of the received pulses from the bicycle reflector array indicate very fine Gaussian-shaped structures. These correspond to the returns from the first few bicycle reflectors within the laser footprint. In addition to the distortions from overlapping, the shapes of these structures are very similar to the returns from the retro-reflector, and it is not clear if there are any speckle noise-induced fluctuations. In order to proceed with the analysis, we hypothetically assume each bicycle reflector to be a retro-reflector (speckle noise-free situation) and try to express the statistics of its returns in a form that we can compare with the experimental results. The analytical result shows that the signal-to-noise ratio of a returned signal from a retro-reflector is given by

$$SNR = \frac{1}{1/\langle N\rangle + \mathrm{var}(\alpha)} \qquad (3)$$

where $\langle N\rangle$ is the mean received energy, and $\alpha$ is a random proportionality factor which includes the fluctuations due to turbulence, laser output, and photomultiplier's gain. In the shot-noise limiting case, the SNR is proportional to the mean received energy. This means that, if there is no speckle noise-induced fluctuation, we expect each SNR plot to be identical to the mean pulse shape. But as the actual SNR plots indicate, the SNR's of the bicycle reflector returns drop off to a negligible level relative to the SNR's of the retro-reflector returns. From the above reasoning, we conclude that there are speckle noise-induced fluctuations in the returns from the bicycle reflector array, and these fluctuations cause the reductions in SNR.

Theoretically, the performance of a correlation algorithm in arrival time estimation is related directly to the returned signal bandwidth, the signal strength, and the number of speckle correlation cells. Since the speckle noise does not have significant contributions to the returned signals in this experiment, we shall neglect its effect on the timing performance.

The returns from the bicycle reflector array contain sharp temporal structures which correspond to high-frequency signals, and the signal strengths are reasonably high due to the specular nature of the small cube-corner reflectors. As a result, we expect reasonably good estimates of arrival times for these returns. On the contrary, the returns from the plate target contain relatively low-frequency contents, and the signal strengths are not as high because of the diffused target surface. Therefore, we do not expect the correlation receiver to perform as well in estimating the arrival times for these returns. This fact is well-illustrated experimentally by referring to the histograms of the arrival-time estimation. The results indicate that the single shot accuracy is 40 to 120 psec for the bicycle reflector configuration, while the single shot accuracy is 90 to 140 psec for the plate target configuration. The timing accuracy of the bicycle reflector configuration is of considerable interest since this configuration simulates the actual ocean surface. By averaging over 100 shots, a timing accuracy of 4 psec is achievable. This corresponds to the pressure measurement accuracy of 2 mbar. Thus, the results show that the pulsed two-color laser altimeter technique in measuring pressure is promising. Further experiments have been planned to verify the feasibility of this

technique for airborne and satellite-based applications.

# 6. CONCLUSIONS

The horizontal path ranging experiment was conducted in March, 1983 to verify the feasibility of the remote pressure measurement technique for weather modeling. The waveforms of the received signals from both the ocean-simulated bicycle reflector array and the range-spread plate target were recorded, and their corresponding arrival times were estimated using the correlation algorithm. For the ocean-simulated bicycle reflector configuration, the atmospheric delay can be measured with an accuracy of 40 psec on each laser pulse. This accuracy permits 4 psec accuracy on 100-shot averages of the receiver data. For the plate target configuration, a timing accuracy of 90 psec on each laser firing is achievable. This corresponds to a 9-psec accuracy on 100-shot averages. In order to acquire higher accuracies which are essential to applications in barometric measurements, a receiver system with better time resolution is required. A streak tube camera-based receiver system of 5-psec time resolution is planned to replace the waveform digitizer-based receiver system. Subsequent airborne experiments using this system are planned in the spring of 1984.

## REFERENCES


[1] P. L. Bender and J.C. Owens, "Correction Of Optical Distance Measurements For The Fluctuating Atmospheric Index Of Refraction," J. Geophys. Res., Vol. 70, 2461, May 1965.

[2] R. W. Agreen and D. E. Smith, "A Simulation Of The San Andreas Fault Experiment," J. Geophys. Res., Vol. 79, 4413, October 1974.

[3] J. W. Siry, "Crustal Motion Measurement By Means Of Satellite Techniques," GSFC Report X-590-73-273, May 1973.

[4] Von Bun et al., "Spaceborne Earth Applications Ranging System," GSFC Report X-920-75-299, December 1975.

[5] C. S. Gardner, "Technique For Remotely Measuring Surface Pressure From A Satellite Using A Multicolor Laser Ranging System," Appl. Opt., Vol. 18, 3184, September 1979.

[6] C. S. Gardner, B. M. Tsai and K. E. Im, "Multicolor Laser Altimeter For Barometric Measurements Over The Ocean : Theoretical," Appl. Opt., Vol. 22, September 1983.

[7] J. B. Abshire, "Pulsed Multiwavelength Laser Ranging System," NASA Memorandum 83917, March 1982.

[8] J. B. Abshire and J. E. Kalshoven, Jr., "Multicolor Laser Altimeter For Barometric Measurements Over The Ocean : Experimental," Appl. Opt., Vol. 22, September 1983.

[9] B. M. Tsai and C. S. Gardner, "Time-Resolved Speckle," to be submitted for publication in Appl. Opt., 1983.

[10] J. W. Goodman, "Some Effects Of Target-Induced Scintillation On Optical Radar Performance," Proc. IEEE, Vol. 53, 1688, November 1965.

CUMULATIVE LIST OF RADIO RESEARCH LABORATORY REPORTS

PREPARED UNDER NASA GRANT NSG-5049

RRL Rep. No. 469 - Gardner, C. S. (December 1975), The Effects of Random Path Fluctuations on the Accuracy of Laser Ranging Systems.

RRL Rep. No. 471 - Zanter, D. L., C. S. Gardner and N. N. Rao (January 1976), The Effects of Atmospheric Refraction on the Accuracy of Laser Ranging Systems.

RRL Rep. No. 477 - Gardner, C. S. and J. R. Rowlett (November 1976), Atmospheric Refraction Errors in Laser Ranging Data.

RRL Rep. No. 478 - Gardner, C. S. and B. E. Hendrickson (December 1976), Correction of Laser Ranging Data for the Effects of Horizontal Refractivity Gradients.

RRL Rep. No. 481 - Gardner, C. S. (January 1977), Statistics of the Residual Refraction Errors in Laser Ranging Data.

RRL Rep. No. 486 - Gardner, C. S. (June 1977), Comparison Between the Refraction Error Covariance Model and Ray Tracing.

RRL Rep. No. 488 - Gardner, C. S. (December 1977), Speckle Noise in Satellite Based Lidar Systems.

RRL Rep. No. 495 - Gardner, C. S. and G. S. Mercherle (April 1978), Speckle Noise in Direct-Detection Lidar Systems.

RRL Rep. No. 496 - Gardner, C. S. and A. M. Saleh (October 1978), Speckle Noise in Differential Absorption Lidar Systems.

RRL Rep. No. 499 - Gardner, C. S. (January 1979), A Technique for Remotely Measuring Surface Pressure from a Satellite Using a Multicolor Laser Ranging System.

RRL Rep. No. 502 - Palluch, E., J. Shelton and C. S. Gardner (May 1979), Operating Manual for the RRL 8 Channel Data Logger.

RRL Rep. No. 505 - Gardner, C. S. and R. Axford, Jr. (March 1980), Regression Models for Multicolor Satellite Laser Ranging.

RRL Rep. No. 510 - Gardner, C. S. (April 1981), Analysis of Target Signatures for Laser Altimeters.

RRL Rep. No. 514 - Tsai, B. and C. S. Gardner (December 1981), Remote Sensing of Sea State by Laser Altimeters.

RRL Rep. No. 518 - Gardner, C. S. (August 1982), Optical Communications.

RRL Rep. No. 519 - Im, K. E. and C. S. Gardner (September 1982), Atmospheric Refraction Effects on Baseline Error in Satellite Laser Ranging Systems.

RRL Rep. No. 526 - Im, K. E., B. M. Tsai and C. S. Gardner (September 1983), Analysis of Short Pulse Laser Altimetry Data obtained over Horizontal Path.

## PAPERS PUBLISHED

C. S. Gardner, "Effects of Random Path Fluctuations on the Accuracy of Laser Ranging Data," Applied Optics, 15, 2539-2545, October 1976.

C. S. Gardner, "Effects of Horizontal Refractivity Gradients on the Accuracy of Laser Ranging to Satellites," Radio Science, 11, 1037-1044, December 1976.

C. S. Gardner, "Correction of Laser Tracking Data for the Effects of Horizontal Refractivity Gradients," Applied Optics, 16, 2427-2432, September 1977.

C. S. Gardner, J. R. Rowlett, and B. E. Hendrickson, "Ray Tracing Evaluation of a Technique for Correcting the Refraction Errors in Satellite Tracking Data," Applied Optics, 17, 3143-3145, October 1978.

C. S. Gardner, "Technique for Remotely Measuring Surface Pressure from a Satellite Using a Multicolor Laser Ranging System," Applied Optics, 18, 3184-3189, September 15, 1979.

C. S. Gardner, "Target Signatures for Laser Altimeters: An Analysis," Applied Optics, 21, 448-453, February 1, 1982.

B. M. Tsai, and C. S. Gardner, "Remote Sensing of Sea State Using Laser Altimeters," Applied Optics, 21, 3932-3940, November 1, 1982.

C. S. Gardner, B. M. Tsai and J. B. Abshire, "Remote Sensing of Atmospheric Pressure and Sea State from Satellites Using Short-Pulse Multicolor Laser Altimeters," Proceedings of NATO-AGARD Symposium on Propagation Factors Affecting Remote Sensing by Radio Waves, Oberammergau, FRG, May 24-28, 1983.

C. S. Gardner, B. M. Tsai and K. E. Im, "Multicolor Laser Altimeters for Barometric Measurements over the Ocean: Theoretical," Applied Optics, 22, September, 1983.